Cell Reports
Article

OPEN ACCESS
CellPress

Phosphorylation of Npas4 by MAPK Regulates Reward-Related Gene Expression and Behaviors

Yasuhiro Funahashi,[1,4] Anthony Ariza,[1,4] Ryosuke Emi,[1] Yifan Xu,[1] Wei Shan,[2] Ko Suzuki,[1] Sachi Kozawa,[1] Rijwan Uddin Ahammad,[1] Mengya Wu,[1] Tetsuya Takano,[1] Yoshimitsu Yura,[1] Keisuke Kuroda,[1] Taku Nagai,[2] Mutsuki Amano,[1] Kiyofumi Yamada,[2] and Kozo Kaibuchi[1,3,5,*]

[1]Department of Cell Pharmacology, Nagoya University Graduate School of Medicine, 65 Tsurumai, Showa, Nagoya 466-8550, Japan
[2]Department of Neuropsychopharmacology and Hospital Pharmacy, Nagoya University Graduate School of Medicine, 65 Tsurumai, Showa, Nagoya 466-8550, Japan
[3]Institute for Comprehensive Medical Science, Fujita Health University, Toyoake, Aichi 470-1192, Japan
[4]These authors contributed equally
[5]Lead Contact
*Correspondence: kaibuchi@med.nagoya-u.ac.jp
https://doi.org/10.1016/j.celrep.2019.10.116

SUMMARY

Dopamine (DA) activates mitogen-activated protein kinase (MAPK) via protein kinase A (PKA)/Rap1 in medium spiny neurons (MSNs) expressing the dopamine D1 receptor (D1R) in the nucleus accumbens (NAc), thereby regulating reward-related behavior. However, how MAPK regulates reward-related learning and memory through gene expression is poorly understood. Here, to identify the relevant transcriptional factors, we perform proteomic analysis using affinity beads coated with cyclic AMP response element binding protein (CREB)-binding protein (CBP), a transcriptional coactivator involved in reward-related behavior. We identify more than 400 CBP-interacting proteins, including Neuronal Per Arnt Sim domain protein 4 (Npas4). We find that MAPK phosphorylates Npas4 downstream of PKA, increasing the Npas4-CBP interaction and the transcriptional activity of Npas4 at the brain-derived neurotrophic factor (BDNF) promoter. The deletion of Npas4 in D1R-expressing MSNs impairs cocaine-induced place preference, which is rescued by Npas4-wild-type (WT), but not by a phospho-deficient Npas4 mutant. These observations suggest that MAPK phosphorylates Npas4 in D1R-MSNs and increases transcriptional activity to enhance reward-related learning and memory.

INTRODUCTION

Dopamine (DA) is important for motor function, motivation, working memory, and the reward system (Girault and Greengard, 2004; Phillips et al., 2008). Functional deficits in DA signaling have been implicated in various neuropsychological diseases, including Parkinson's disease, drug addiction, compulsive behavior, autism spectrum disorders, and schizophrenia (Carlsson, 2001; Hyman et al., 2006; Iversen and Iversen, 2007; Koob and Volkow, 2010; Swanson et al., 2007). Experiencing reward and using various drugs of abuse, such as cocaine or methamphetamine, activate intracellular pathways in the brain reward system, including the ventral tegmental area (VTA), the nucleus accumbens (NAc), and the prefrontal cortex (Rogge and Wood, 2013). These pathways regulate the expression of genes that are essential for long-lasting forms of synaptic plasticity, memory processes, and drug-induced neuronal and behavioral changes (McClung and Nestler, 2008; Renthal and Nestler, 2008). Despite this knowledge, our current understanding of the mechanisms by which some transcriptional factors (TFs) are stimulated by DA and how they regulate several genes that are important for synaptic plasticity remains incomplete. It is even less well-understood how the changes that occur at the intracellular level manifest in behavioral changes.

The principal target of DA is medium spiny neurons (MSNs), which are a special type of GABAergic inhibitory cell that comprises 90% of the neurons within the striatum, including the NAc. The MSNs in the NAc receive inputs from the dopaminergic neurons of the VTA and the glutamatergic neurons of the hippocampus, amygdala, and medial prefrontal cortex. There are two distinct classes of spatially intermixed MSNs that express dopamine type 1 or 2 receptors (D1R-MSNs or D2R-MSNs, respectively; Smith et al., 2013). D1R-MSN and D2R-MSN subpopulations were also originally characterized as direct and indirect pathways in the dorsal striatum. D1R is coupled to adenylate cyclase through G_{olf} (G_s) and activates protein kinase A (PKA), whereas D2R inhibits adenylate cyclase through G_i (Hervé et al., 1993; Stoof and Kebabian, 1984). We previously found that DA stimulates Rap1 GEF (Rasgrp2) phosphorylation via PKA in D1R-MSNs, thereby activating Rap1, and then Rap1 regulates neuronal excitability and behavioral responses to cocaine reward through mitogen-activated protein kinase 1/3 (MAPK1/3), also known as extracellular-signal-regulated kinase 1/2 (ERK1/2) (Nagai et al., 2016). MAPK1/3 is thought to phosphorylate several potassium and HCN channels that are potentially involved in neuronal excitability (Nagai et al., 2016). Alternatively, MAPK1/3 may phosphorylate several nuclear TFs that are involved in gene expression, long-term synaptic plasticity, and

This is an open access article under the CC BY-NC-ND license (http://creativecommons.org/licenses/by-nc-nd/4.0/).

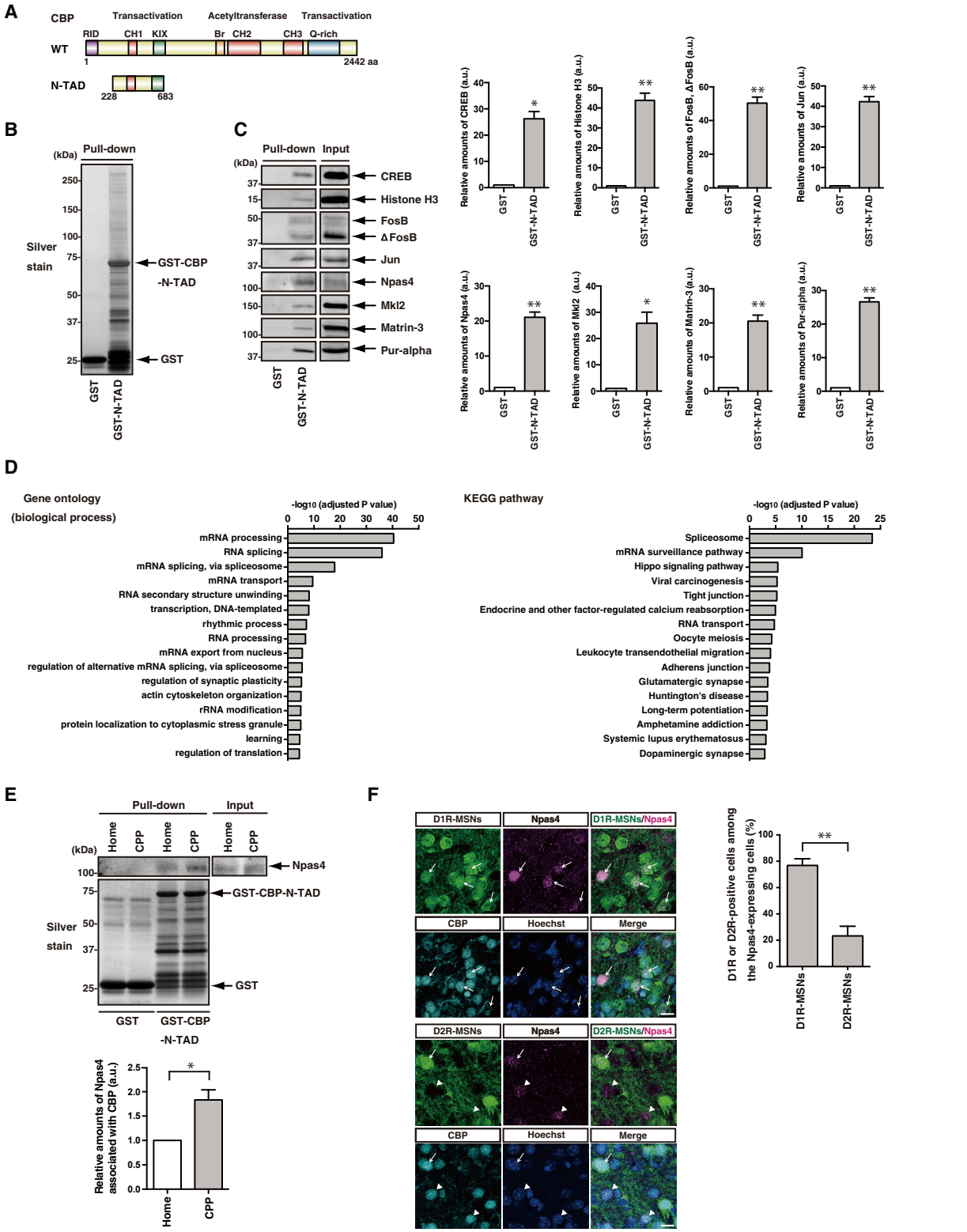

Figure 1. Npas4 Is a Novel CBP-Interacting Protein

(A) Schematic representation of CBP. The domain organization of CBP and CBP-N-TAD is represented. The numbers indicate amino acids. Br, Bromo domain; CH-1, CH-2, CH-3, cysteine-histidine-rich domains 1–3; KIX, kinase-inducible interaction domain; N-TAD, N-terminal transactivation domain; Q-rich, glutamine-rich domain; RID, nuclear receptor interaction domain.

(legend continued on next page)

memory formation. However, it remains unclear how MAPK1/3 regulates gene expression and memory formation downstream of the D1R/PKA/Rap1 pathway.

TFs such as c-Fos, FosB, and cyclic AMP response element (CRE) binding protein (CREB) are activated by DA and mediate the expression of genes that are involved in synaptic plasticity (Hyman and Malenka, 2001; Nestler, 2001; Robinson and Kolb, 1999). A variety of protein kinases, including PKA, RSK, and CaMKII, activate CREB via serine-133 (S133) phosphorylation (Choe and McGinty, 2000, 2001; Dash et al., 1991; Montminy et al., 1990; Sheng et al., 1991; Xing et al., 1996, 1998). The phosphorylation of CREB at S133 recruits CREB-binding protein (CBP) to promote transcription. CBP and its homolog p300 are essential transcriptional coactivators for many TFs (Karamouzis et al., 2007; Vo and Goodman, 2001). CBP/p300 can also act as a scaffold protein, stabilizing the transcription complex by simultaneously binding to other proteins. CBP also regulates transcription during memory and synaptic plasticity (Barrett and Wood, 2008). The deletion of CBP in the NAc correlates with impairments in cocaine sensitivity and reward-related learning and memory (Malvaez et al., 2011; Rogge and Wood, 2013). However, how CBP cooperates with many TFs during reward-related memory processing is not fully understood.

Here, we isolated and concentrated TFs from the mouse striatum using affinity beads coated with CBP, which acts as a transcriptional coactivator, and identified several TFs, including Neuronal Per Arnt Sim domain protein 4 (Npas4). MAPK phosphorylated Npas4 downstream of PKA. The phosphorylation of Npas4 increased the interaction between Npas4 and CBP, thereby regulating transcriptional activity to enhance reward-related learning and memory.

RESULTS

Proteomic Analysis of CBP-Binding Proteins

To concentrate and identify TFs that are associated with reward-related learning and memory, we subjected mice to cocaine-induced conditioned place preference (CPP) conditioning and performed a glutathione-S-transferase (GST) pull-down assay followed by shotgun analysis using liquid chromatography-tandem mass spectrometry (LC-MS/MS). CPP is a behavioral paradigm based on the principles of Pavlovian conditioning (Tzschentke, 2007). In the conditioning session of the CPP, mice learn to associate the rewarding effects of cocaine to a neutral environmental context that has been paired with cocaine administration. We injected cocaine into mice and placed them into the CPP test chamber for 30 min, after which nuclear extracts from the striatal region, including the NAc, were applied to affinity beads coated with GST or the GST-CBP-N-terminal transactivation domain (N-TAD), which can interact with several TFs, such as CREB (Karamouzis et al., 2007; Vo and Goodman, 2001; Figure 1A). Numerous proteins were eluted from the affinity beads coated with GST-CBP-N-TAD, whereas fewer proteins from affinity beads coated with GST (Figure 1B). The bound proteins were digested using trypsin/Lys-C and subjected to LC-MS/MS to identify interacting proteins. By the shotgun analysis, we identified more than 400 proteins that specifically interact with GST-CBP-N-TAD, but not with GST (Tables 1 and S1). To confirm the results obtained in the proteomic analysis, we performed an immunoblot analysis using specific antibodies. CREB, Histone H3, FosB, ΔFosB, and Jun interacted with GST-CBP-N-TAD, but not GST, as previously described (Figure 1C; Parker et al., 1996; Tsai et al., 2008; Vo and Goodman, 2001). CBP-interacting candidates, including Npas4, MKL/myocardin-like protein 2 (Mkl2), Matrin-3, and transcriptional activator protein Pur-alpha (purine-rich element-binding protein alpha), also specifically interacted with GST-CBP-N-TAD, but not GST (Figure 1C). To investigate the functions of the identified CBP-interacting proteins, we performed gene ontology (GO) analysis (biological process) and KEGG (Kyoto Encyclopedia of Genes and Genomes) pathway analysis using the DAVID bioinformatics resources (Huang da et al., 2009a, 2009b). We found that most CBP-interacting proteins were classified into RNA and transcription-related proteins, and some were also classified into synaptic plasticity and learning-related proteins in GO analysis (Figure 1D). KEGG pathway analysis showed that the CBP-interacting proteins were involved not only in spliceosome and mRNA surveillance but also in long-term potentiation, amphetamine addiction, and dopaminergic synapse (Figure 1D).

Among the CBP-interacting candidates in the categories of synaptic plasticity and learning, further experiments focused on Npas4. Npas4 is a brain-specific basic helix-loop-helix transcriptional factor that is expressed throughout the whole brain at a low level in the resting state, though it is enriched in the limbic system, such as the hippocampus, amygdala, and NAc (Choy et al., 2015; Leong et al., 2013; Ooe et al., 2004). Npas4 plays a role in the expression of activity-dependent genes, such as c-Fos and brain-derived neurotrophic factor (BDNF)

(B) Identification of CBP-interacting proteins. After CPP conditioning, the nuclear fraction of the mouse brain lysate from the striatum and NAc was loaded onto beads coated with GST or GST-CBP-N-TAD. Aliquots of the eluate were resolved by SDS-PAGE, followed by silver staining.

(C) Validation of the results of the proteomic analysis. The eluates from GST and GST-CBP-N-TAD columns were analyzed by immunoblotting using anti-CREB, anti-Histone H3, anti-FosB, anti-Jun, anti-Npas4, anti-Mkl2, anti-Matrin-3, and anti-Pur-alpha antibodies. The data represent the mean ± SEM of three independent experiments. *$p < 0.05$; **$p < 0.01$.

(D) GO analysis (biological process) and KEGG pathway analysis of CBP-interacting proteins using DAVID bioinformatics resources.

(E) The interaction between Npas4 and CBP after CPP conditioning. After CPP conditioning, the brain lysate from the striatum and NAc was loaded onto beads coated with GST or GST-CBP-N-TAD. Aliquots of the eluate were resolved by SDS-PAGE, followed by silver staining (bottom) or immunoblotting with anti-Npas4 antibody (top). The data represent the mean ± SEM of three independent experiments. *$p < 0.05$. Home, home cage.

(F) Colocalization of Npas4 and CBP in D1R-MSNs or D2R-MSNs after CPP conditioning. Coronal brain slices were immunostained with anti-GFP, anti-Npas4, and anti-CBP antibodies. Nuclei were visualized with Hoechst 33342. Arrows indicate D1R- or D2R-positive cells among the Npas4-expressing cells. Arrowheads indicate D2R-negative cells among the Npas4-expressing cells. The scale bars represent 10 μm. The data plot shows the percentage of D1R- or D2R-positive cells among the Npas4-expressing cells in the NAc. At least 30 cells per sample were measured. The data represent the mean ± SEM of three independent experiments. **$p < 0.01$.

Table 1. List of Identified CBP-Interacting Proteins

Akap5	Akap8	Kiaa1210	Ablim2	Arf3	Actn1	Actn2	Actn4
Add1	Apba2	Anks1b	Ankrd63	Ank2	Ank3	Ap2a1	Ap2a2
Ap2b1	Ap2m1	Amer2	Agap2	Ahdc1	Atp5c1	Pfkp	Dhx9
Ddx1	Ddx18	Ddx3x	Ddx3y	Ddx50	Dhx36	Atad3	Aurkaip1
Epb41l3	Add2	No66	Bmp1	Baiap2	Bcan	Brd7	Brd9
Btbd17	Kctd16	Mapk8ip3	Cdh2	Calcoco1	Slc25a12	Calm1	Camsap3
Calu	Camkv	Csnk1e	Csnk2a1	Clpb	Caap1	Ctnna1	Ctnna2
Ctnnb1	Ctnnd2	Ctif	Cdc5l	Cenpv	Pde2a	Cspg5	Chtop
Cbx3	Cbx6	Chd4	Chd5	Cltc	Cldn11	Clvs2	Cpsf1
Cpsf2	Cpsf3	Cpsf4	Ccdc136	Csde1	Cirbp	C3	C1qbp
Cnksr2	Fam120b	H2afy	H2afy2	Coro1c	Coro2b	Ckmt1	Creb1
Cdk12	Cyb561d1	Cyth3	Cyfip2	Cpeb2	Cpeb3	Specc1	Dbp
Bdh1	Znf326	Dgkb	Dgkz	Tfb1m	Dlg2	Dlg3	Dlgap3
Polr2b	Polr2e	Dnaja	Dnaja3	Dnajc10	Adarb1	Dynll1	Dynll2
Mib2	Nedd4	Smurf1	Egr3	Entpd4	Elavl1	Elavl3	Slc4a4
Tufm	Ngef	Esrp1	Erc2	Eif4a3	Slc1a2	Capza1	Capza2
Capzb	Fbxo3	Fbxo41	Fbxw10	Fez1	Farp1	Fbln5	Fmr1
Fxr1	Fxr2	Fn3k	Aldoa	Fyco1	Grsf1	Gtf3c1	Gtf3c5
Gtf3c5	Grin2b	Grwd1	Glul	Glrx2	Gnb2l1	Gnb4	Gnb5
Gar1	Dkc1	Hspa12a	Hp1bp3	Hnrnpab	Hnrnpa0	Hnrnpa1	Hnrnpdl
Hnrnpdl	Hnrnpm	Syncrip	Hnrnpu	Hnrnpul1	Hnrnpul2	Hnrnpc	Hk1
H1f0	Hist1h1c	Hist1h1e	Hist2h2ac	Hist1h2bf	H3f3c	Hist1h4a	Rbbp4
Kmt2a	Homer1	Kpnb1	Usp53	Ing2	Ints3	Itgb1bp1	Ilf2
Ilf3	Aqr	Iqsec1	Iqsec2	Isca2	Jup	Khdrbs1	Khdrbs2
Khdrbs3	Kif2a	Lmnb1	Lgi1	Lgi2	Lgi3	Lrrc7	Cd47
Ppfia2	Ppfia3	Ssb	Ccm2	Map6d1	Map7d1	Matr3	Grm1
Mbd3	Mgst3	Map1b	Map4	Mapre3	Map1lc3a	Mast3	Slc25a11
Mtfr1l	Timm50	Mapk1	Mkl1	Mkl2	Mybbp1a	Myef2	Mag
Mog	Mlf2	Myl12b	Myh10	Myh9	Sbf1	Cmas	Naa30
Nwd2	Nckap1	Ntn1	Ppp1r9b	Nrxn1	Nfasc	Npas4	Nhp2l1
Nono	Nfic	Nfatc4	Nup133	Nup160	Nup85	Ncor2	Nxf1
Exog	Ybx1	Nop16	Nop56	Nop58	Ddx21	Ncl	Nup43
Nupl2	Ptcd3	Ppil1	Cask	Slc25a3	Pi4ka	Pip5k1a	Pacs1
Pkp4	Plrg1	Pabpn1	Poldip2	Kcna1	Kcnq2	Wdr33	Prpf19
Prpf8	Bcas2	Ddx17	Ddx27	Ddx6	Ythdc2	Dimt1	Smarca2
Rbm19	Usp9x	Phb2	Akt1s1	Prr3	Lrp1	Psma8	Bsn
Pdia4	Emsy	Fam131b	Fam98a	Fam98b	Fosb	Prkcb	Prkcg
Lin7c	Magoh	Pptc7	Ik	Rufy3	Soga3	Sec31b	Unc13a
Wiz	Purg	Glyr1	Dhx15	Rapgef4	G3bp2	Rap1a	Ptprs
Rims1	Rgs9	Rcn2	Arhgef2	Rhog	Prps1	Rsl1d1	Rrs1
Rpf2	Rimbp2	Rbfox1	Rbfox3	Rbm10	Rbm14	Rbm4b	Rbm7
Rbm8a	Fus	Msi2	Raly	Fbl	Fbll1	Ruvbl1	Ruvbl2
Skp1	Sarnp	Atp2a2	Safb2	Sept7	Strap	Srrm2	Mark2
Cdc42bpa	Cdc42bpb	Sik3	Ppp2r2a	Ppp2r2d	Ppp2r2c	Ppp2r1a	Ppp6c
Ppp6r3	Ppp1ca	Shank3	Scoc	Sfxn3	Snrpe	Snrpf	Snrpg
Snrpd1	Snrpn	Snw1	Atp1a1	Atp1a3	Atp1b1	Slc2a	Slc25a48
Sorbs2	Strbp	Ddx39b	Sf3a1	Sf3b1	Sf3b3	Sf3b4	Sf3b6
Sfpq	Srcin1	Srpk1	Srpk2	Hspa9	Stip1	Strn4	Strip2
Sdha	Sdhb	Sucla2	Sun1	Surf6	Sugp2	Smarcb1	Synpo
Snap25	Syt7	Snph	Tardbp	Tnr	Tns2	Zcchc6	Spock2

(*Continued on next page*)

Table 1. *Continued*

Alyref	Thy1	Tef	Tjp1	Tjp2	Smarca4	Eny2	Jun
Pura	Purb	Ctcf	Tra2a	Tgfb1i1	Slc25a1	Trim3	Trim46
Trio	Rtcb	Tmod1	Tmod2	Tmod3	Tmod4	Tubal3	Tinagl1
Baz1b	Snrpc	Snrpa1	Prpf3	Snrnp200	Snrnp40	Fyttd1	Usp46
Rps27a	Gm996	Myo5a	Cn166	Ubp1	Hacd3	Vdac1	Vdac2
Vdac3	Kcnab2	Wdr37	Wdr47	Wdr6	Wdr7	Wdr82	Smu1
Zbtb7a	Zc3h11a	Zc3h4	Zcrb1	Zmat4	Znf148	Znf281	Znf512
Znf638	Znf771	Zfr	Eftud2	Ywhab	Ywhae	Ywhah	Ywhag
Ywhaq	Ywhaz	Ogdh					

The nuclear extracts of the striatal and NAc were applied to affinity beads coated with GST or GST-CBP-N-TAD. The bound proteins were digested using trypsin/Lys-C and subjected to LC-MS/MS to identify the proteins. To select proteins that specifically interact with CBP, the proteins from the control GST column were removed from the data. High-abundance proteins (such as keratin and ribosomal protein) were also excluded.

to control synaptic plasticity (Bloodgood et al., 2013; Lin et al., 2008; Pruunsild et al., 2011; Ramamoorthi et al., 2011; Spiegel et al., 2014). Npas4 is also required for normal social interaction and contextual memory formation in mice (Coutellier et al., 2012; Ramamoorthi et al., 2011). We examined whether CPP conditioning would affect the interaction between CBP and Npas4 and found that the interaction increased after CPP conditioning (Figure 1E). It has been reported that Npas4 was expressed in multiple cell types, including MSNs, in the NAc (Taniguchi et al., 2017). However, it is unknown whether Npas4 is expressed in D1R-MSNs or D2R-MSNs. To provide more accurate information of Npas4 expression in MSNs, we compared the expression of Npas4 in Drd1-mVenus and Drd2-mVenus transgenic mice that were injected with cocaine and placed into the CPP chamber. We found that more than 75% of Npas4-expressing cells were D1R-MSNs positive, and less than 25% of Npas4-expressing cells were D2R-MSNs positive in the NAc (Figure 1F). Npas4 colocalized with CBP in the nuclei (Figure 1F). These results suggest that Npas4 associates with CBP in the nuclei of D1R-MSNs in the NAc under CPP conditioning.

MAPK Regulates the Interaction between CBP and Npas4

To examine the Npas4-binding region of CBP, we transfected GFP-Npas4-wild-type (WT) into COS7 cells and performed a GST pull-down assay using various GST-CBP fragments as bait. Npas4 mainly bound to the N-TAD (228–683 amino acids [aas]) of CBP. Npas4 weakly bound to the C-TAD (1,891–2,442 aas), but not to the nuclear receptor interaction domain (RID) (1–227 aas), the Bromo (684–1,172 aas), or the histone acetyltransferase (HAT) (1,173–1,890 aas) domains (Figures 2A and 2B). To examine the CBP-binding region of Npas4, we transfected Myc-CBP-N-TAD into COS7 cells and performed a GST pull-down using various GST-Npas4 fragments as bait. CBP mainly bound to the TAD (598–802 aas) of Npas4. CBP weakly bound to the middle domain (274–597 aas), but not to the basic helix-loop-helix (bHLH)-Per Arnt Sim (PAS) domain (1–273 aas; Figures 2C and 2D). These results indicate that the N-TAD domain of CBP mainly binds to Npas4 274–802 aas.

It has been reported that the kinase-inducible interaction (KIX) domain of CBP, which is located in the CBP-N-TAD, interacts with the kinase-inducible domain (KID) of CREB and that this interaction is increased by the phosphorylation of CREB at S133 (Chrivia et al., 1993). Thus, we speculated that the interaction between CBP and Npas4 was also regulated by phosphorylation. To examine whether the phosphorylation of Npas4 modulates its interaction with CBP, we performed a GST pull-down assay using okadaic acid (OA), a phosphatase inhibitor, to increase Npas4 phosphorylation. We also used specific inhibitors for several kinases, including MAP2K (MEK), c-*jun* N-terminal kinase (JNK), p38 MAPK, glycogen synthase kinase-3 (GSK3), PKA, and phosphoinositide 3-kinase (PI3K). These kinase inhibitors specifically inhibited OA-induced phosphorylation of each kinase substrate (Figure S1). The treatment of GFP-Npas4-WT-expressing COS7 cells with OA induced a band shift of GFP-Npas4-WT and increased the interaction between GFP-Npas4-WT and GST-CBP-N-TAD, and this interaction was inhibited by U0126 (MAP2K inhibitor), but not by SP600125 (JNK inhibitor), SB203580 (p38 MAPK inhibitor), SB216763 (GSK3 inhibitor), H89 (PKA inhibitor), and LY294002 (PI3K inhibitor; Figure 2E). We also found that the cotransfection of the constitutively active (CA) form of MAP2K1 into COS7 cells induced a band shift of GFP-Npas4-WT and increased its interaction with GST-CBP-N-TAD, although neither MAP2K1-WT nor the dominant-negative (DN) form of MAP2K1 showed such effects (Figure 2F). These results suggest that MAPK phosphorylates Npas4 and, consequently, increases its interaction with CBP.

Identification of Sites Where MAPK Phosphorylates Npas4

Next, we examined whether MAPK directly phosphorylates Npas4. An *in vitro* phosphorylation assay revealed that MAPK1 effectively phosphorylated Npas4 274–597 aas and 598–802 aas, but not 1–273 aas (Figures 3A and 3B), suggesting that MAPK1 directly phosphorylates Npas4 274–802 aas *in vitro*. To further investigate whether MAPK phosphorylates Npas4 in COS7 cells, we performed Phos-tag SDS-PAGE, in which phosphorylated protein has a slower migration rate on

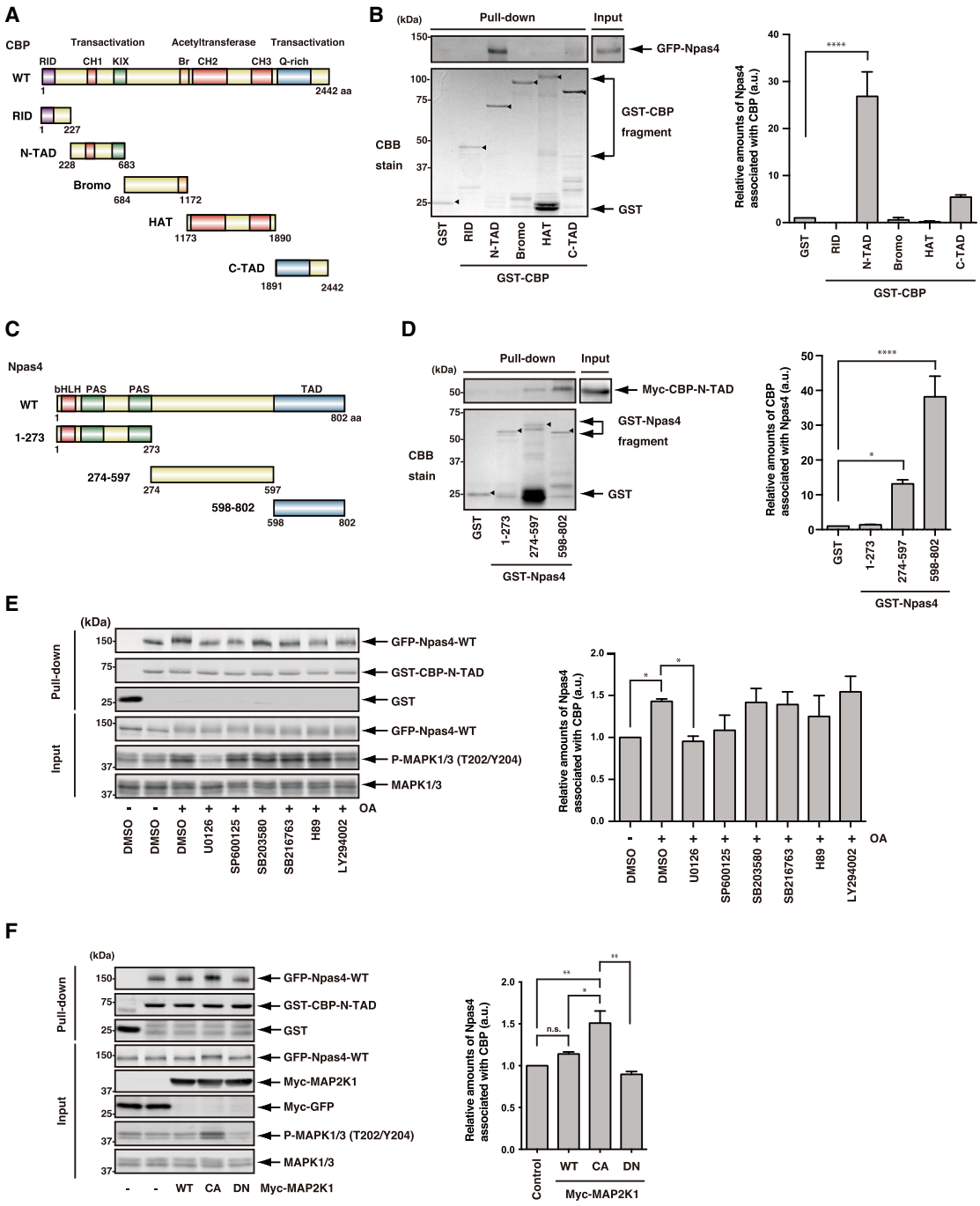

Figure 2. MAPK Regulates the Interaction between CBP and Npas4

(A) Schematic representation of CBP. The domain organization of CBP-WT, RID, N-TAD, Bromo, HAT, and C-TAD is represented. The numbers indicate amino acids. HAT, histone acetyltransferase.

(B) The Npas4-binding domain of CBP. COS7 cells were cotransfected with GFP-Npas4-WT. Extracts of COS7 cells were incubated with glutathione beads coated with 100 pmol of GST or GST-CBP fragments. The bound proteins were subjected to immunoblot analysis using an anti-GFP antibody and Coomassie Brilliant Blue (CBB) staining. Arrowheads indicate intact GST-fusion proteins. The data represent the mean ± SEM of three independent experiments. ****$p < 0.0001$.

(C) Schematic representation of Npas4. The numbers indicate amino acids. bHLH, basic helix-loop-helix; PAS, Per Arnt Sim domain; TAD, transactivation domain.

(legend continued on next page)

the gel as compared to nonphosphorylated proteins (Kinoshita et al., 2006). GFP-Npas4-WT was prominently shifted upward when GFP-Npas4-WT was coexpressed with MAP2K1-CA, but not with MAP2K1-WT or DN (Figure 3C), indicating that Npas4 is phosphorylated by MAPK in COS7 cells. To determine which region of Npas4 is phosphorylated by MAPK in COS7 cells, we divided Npas4 274–802 aas into five fragments: Npas4 274–389 aas; 390–489 aas; 490–597 aas; 598–701 aas; and 702–802 aas (Figure 3A). Npas4 390–489 aas, 490–597 aas, and 598–701 aas appeared as several bands (Figure 3D), and these bands were strongly shifted upward in the presence of MAP2K1-CA. In contrast, neither Npas4 274–389 aas nor Npas4 702–802 aas showed any upward shift when coexpressed with MAP2K1-CA (Figure 3D). These results indicate that MAPK phosphorylation sites exist in Npas4 390–701 aas. To identify the phosphorylation sites of Npas4, pulled down GST-Npas4 fragments coexpressed with MAP2K1-CA from COS7 cells were digested with trypsin/Lys-C at the C terminus of lysine and arginine residues or Glu-C/Asp-N at the C terminus of glutamic acid residues and N terminus of aspartic acid residues and then peptides were analyzed by LC-MS/MS. Dual-phosphorylated peptide DLVCTPPYTPHQPGG CAFLFSLHEPFQTHLPPPSSSLQE, containing T423 and T427 phosphorylation sites, was identified from digested fragments of GST-Npas4-390–489 aas; LPPSPSSPGNGDCTLLALAQLR, containing S577 and S580 phosphorylation sites, was identified from digested fragments of GST-Npas4 490–597 aas; and GLLTPEASPVKQSFFHYTEKE, containing T611 and S615 phosphorylation sites, was identified from digested fragments of GST-Npas4 598–701 aas (Figure S2). Selected ion monitoring (SIM) analysis revealed that the amount of this dual phosphorylation was significantly increased by coexpression with MAP2K1-CA (Figure 3E). To confirm the phosphorylation sites identified by mass spectrometry, we constructed alanine (Ala) mutants of all the (S/T)P sites in the Npas4 fragments and expressed them in COS7 cells with or without coexpression with MAP2K1-CA. The band shifts of Npas4 390–489 aas induced by coexpression with MAP2K1-CA were lost in the T423A/T427A mutant (Figure 3F). The band shifts of Npas4 490–597 aas induced by coexpression with MAP2K1-CA were lost in the S577A/S580A mutant (Figure 3G). The top band shift of Npas4 598–701 aas among the three bands induced by coexpression with MAP2K1-CA was lost in the T611A/S615A mutant (Figure 3H). To confirm the phosphorylation of these sites in full length of Npas4-WT, we mutated T423, T427, S577, S580, T611, and S615 to Ala, producing what we designated the Npas4-6A mutant. The MAPK-dependent band shift of Npas4 was decreased in the Npas4-6A mutant (Figure 3I). Taken together, these results indicate that Npas4 is phosphorylated by MAPK at T423, T427, S577, S580, T611, and S615 sites.

Phosphorylation of Npas4 by MAPK in Striatal Neurons

MAPK is a proline-directed kinase, meaning that it phosphorylates a consensus motif of serine-proline (SP) or threonine-proline (TP). Among the phosphorylation sites of Npas4, T427, S577, and S580 completely match the consensus motif P-X-S/T-P (where X represents any amino acid); T423, T611, and S615 match the consensus motif S/T-P. T423 and T427 are located near the putative docking site for MAPK, known as the DEF domain (docking site for ERK and FXF) (Figure 4A). These phosphorylation sites are well conserved in mammals (human, mouse, and rat; Figure 4A). To monitor the phosphorylation state of Npas4 by MAPK, we prepared antibodies that specifically recognized Npas4 phosphorylated at T427, S577, S580, and S615 (anti-pT427, anti-pS577, anti-pS580, and anti-pS615 antibodies), but we failed to prepare antibodies to recognize Npas4 phosphorylated at T423 and T611. The specificity of these antibodies was examined with immunoblot analysis. GST-Npas4 274–597 aas or GST-Npas4 598–802 aas phosphorylated by MAPK *in vitro* was specifically detected by the anti-pT427, anti-pS577, anti-pS580, and pS615 antibodies in a dose-dependent manner (Figure S3). We also confirmed that the anti-pT427, anti-pS577, anti-pS580, and pS615 antibodies did not cross-react with nonphosphorylated Npas4 (Figure S3).

To examine whether MAPK phosphorylates Npas4 at T427, S577, S580, and S615 in COS7 cells, GFP-Npas4-WT was transfected into COS7 cells with or without the coexpression of MAP2K1-CA. Coexpression with MAP2K1-CA induced the phosphorylation of Npas4 at T427, S577, S580, and S615 (Figure 4B). We confirmed that the anti-pT427, anti-pS577, anti-pS580, and anti-pS615 antibodies did not cross-react with the Npas4-6A mutant and the Npas4 point mutant (Figures 4B and S4). Because the pT427 antibody is the most sensitive, in the following experiment, the pT427 antibody was used to monitor intracellular phosphorylation. The treatment of COS7 with OA induced the phosphorylation of not only MAPK1/3 but also Npas4 at T427 (Figure 4C). The pretreatment of the cells with U0126 inhibited the OA-induced phosphorylation of Npas4 at T427 (Figures 4C and S1), whereas the pretreatment with JNK, p38 MAPK, GSK3, PKA, and PI3K inhibitors did not inhibit the OA-induced phosphorylation of Npas4 at T427 in COS7 cells (Figure S1). These results suggest that MAPK specifically phosphorylates Npas4 at T427 in COS7 cells. To explore Npas4 phosphorylation under more physiologically

(D) The CBP-binding domain of Npas4. COS7 cells were transfected with Myc-CBP-N-TAD. Extracts of COS7 cells were incubated with glutathione beads coated with 100 pmol of GST or GST-Npas4 fragments. The bound proteins were subjected to immunoblot analysis using an anti-Myc antibody and CBB staining. Arrowheads indicate intact GST-fusion proteins. The data represent the mean ± SEM of three independent experiments. *$p < 0.05$; ****$p < 0.0001$.
(E) A MAP2K1 inhibitor decreased CBP-Npas4 binding. COS7 cells were cotransfected with GST or GST-CBP-N-TAD and GFP-Npas4-WT. Cells were pretreated with the indicated inhibitors for 30 min, followed by OA for 1 h. Extracts of COS7 cells were incubated with glutathione beads. The bound proteins were subjected to immunoblot analysis using an anti-GFP and anti-GST antibodies. The data represent the mean ± SEM of three independent experiments. *$p < 0.05$.
(F) MAP2K1-CA increases CBP-Npas4 binding. GFP-Npas4-WT was expressed in COS7 cells with coexpression of Myc-GFP, Myc-MAP2K1-WT, -CA, or -DN. Extracts of COS7 cells were incubated with glutathione beads coated with 100 pmol of GST or GST-N-TAD. Immunoblot analysis was performed using anti-GFP, anti-Myc, anti-GST, anti-pMAPK1/3, and anti-MAPK1/3 antibodies. The data represent the mean ± SEM of three independent experiments. *$p < 0.05$; **$p < 0.01$.

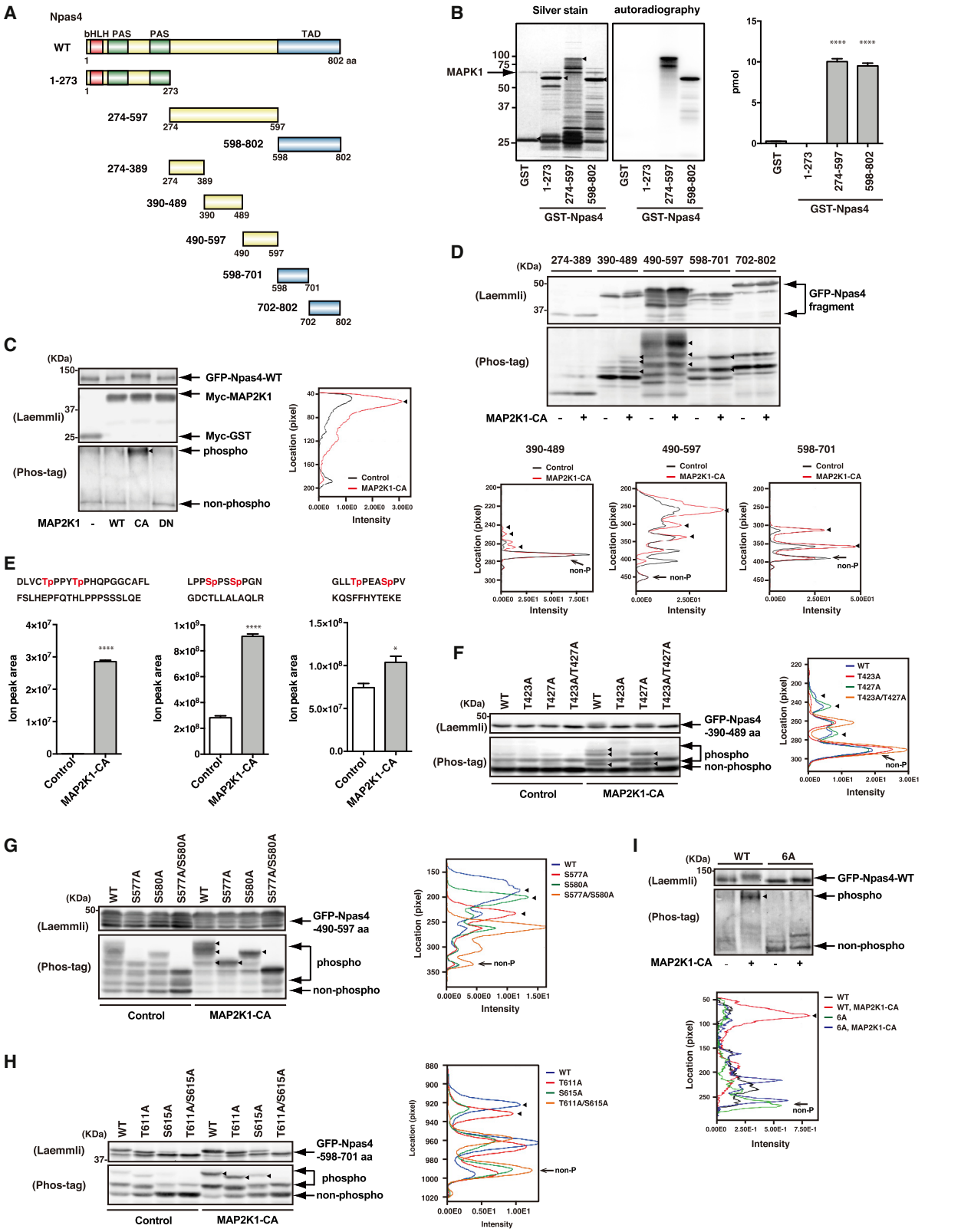

(legend on next page)

relevant conditions, we used cultured striatal neurons. It has been reported that Npas4 protein expression can be induced in cultured neurons by depolarization (50 mM KCl treatment; Lin et al., 2008). Because Npas4 expression levels are very low under normal conditions, it is difficult to detect the endogenous phosphorylation of Npas4. Thus, we pretreated cells with KCl for 1 h to increase Npas4 expression. It has been reported that activation of MAPK by depolarization peaks at 5 min and returns to steady state after 1 to 2 h (Tyssowski et al., 2018). The stimulation of striatal neurons with OA induced the phosphorylation of not only MAPK1/3 but also endogenous Npas4 at T427 (Figure 4D). The pretreatment of the cells with U0126 inhibited the OA-induced phosphorylation of Npas4 (Figure 4D). We previously reported that the treatment of striatal neurons with forskolin (FSK), which specifically produces cyclic AMP (cAMP) and subsequent activation of PKA, increases Rap1 GEF (Rasgrp2) phosphorylation via PKA, and the phosphorylation of Rasgrp2 leads to Rap1 activation, followed by recruitment of the MAPK pathway (Nagai et al., 2016). The stimulation of striatal neurons with FSK induced the phosphorylation of not only Rasgrp2 and MAPK1/3 but also endogenous Npas4 at T427 (Figure 4E). The pretreatment of the cells with U0126 inhibited the FSK-induced phosphorylation of both MAPK1/3 and Npas4, but not Rasgrp2. These results suggest that MAPK phosphorylates Npas4 downstream of the cAMP/PKA/Rap1 pathway (Figure 4E).

Next, we investigated the spatial distribution of phosphorylated Npas4. Unfortunately, the anti-pT427 antibody could not detect the phosphorylation of endogenous Npas4 during immunostaining of the striatal neurons. Accordingly, GFP-Npas4-WT was transfected into cultured striatal neurons to visualize Npas4 and its phosphorylated form. GFP-Npas4-WT was abundantly distributed in the nucleus and also distributed in the cell body (Figure 4F). The stimulation of striatal neurons with FSK induced the phosphorylation of GFP-Npas4-WT at T427 in the nuclei (Figure 4F). Taken together, these results suggest that Npas4 is phosphorylated by MAPK downstream of the cAMP/PKA/Rap1 pathway in the nuclei of cultured striatal neurons.

The Effects of Npas4 Phosphorylation on Its Interaction with CBP; Npas4 Phosphorylation Regulates Transcriptional Activity

To examine whether the MAPK-mediated phosphorylation of Npas4 affects its interaction with CBP, we performed a GST pull-down assay using COS7 cells expressing GFP-Npas4-WT or Npas4-6A. The stimulation of the COS7 cells with OA increased the interaction between GST-CBP-N-TAD and GFP-Npas4-WT, but not with Npas4-6A (Figure 5A). To mimic the phosphorylation of Npas4 by MAPK, we substituted glutamic acid for T423, T427, S577, S580, T611, and S615 to produce GFP-Npas4-6E. GST-CBP-N-TAD interacted with GFP-Npas4-6E more than with GFP-Npas4-WT (Figure 5B). These results suggest that the phosphorylation of Npas4 by MAPK increases its interaction with CBP in COS7 cells.

To measure the transcriptional activity of Npas4, we performed one-hybrid analysis using a luciferase reporter driven by the Gal4-responsive element (Gal4-UAS) and Gal4 DNA-binding domain fused with Npas4 274–802 aas (Gal4-DBD-Npas4 274–802 aas). The transcriptional activity of Npas4 274–802 aas was significantly enhanced by MAP2K1-CA coexpression, as well as FSK treatment (Figure 5C), suggesting that the Npas4 activity was increased downstream of PKA/Rap1/MAPK pathway. It has been reported that Npas4 regulates the expression of several genes, such as *Bdnf*, that are important for neuronal survival and synaptic plasticity (Lin et al., 2008; Pruunsild et al., 2011; Spiegel et al., 2014; Yun et al., 2013). BDNF plays a crucial role in synaptic plasticity and memory processing in the adult brain (Bekinschtein et al., 2008). The levels of *Bdnf* mRNA are increased in the NAc following acute and repeated

Figure 3. Identification of Sites of MAPK-Dependent Npas4 Phosphorylation

(A) Schematic representation of Npas4. The numbers indicate amino acids.

(B) The direct phosphorylation of Npas4 by MAPK1. Purified GST or GST-Npas4 fragments were incubated with recombinant MAPK1 in the presence of [γ- 32P] ATP *in vitro*. Samples were subjected to SDS-PAGE and silver staining followed by autoradiography. Arrowheads indicate intact GST-fusion proteins. Arrow indicates recombinant MAPK1. Data represent the mean ± SEM of three independent experiments. ****$p < 0.0001$.

(C) COS7 cells were cotransfected with GFP-Npas4-WT and Myc-MAP2K1-WT, -CA, or -DN. The cell lysates were analyzed by immunoblotting with anti-GFP and anti-Myc antibodies after Laemmli's SDS-PAGE (upper panel) or Phos-tag SDS-PAGE (lower panel). Arrowhead indicates MAP2K1-dependent phosphorylated bands of GFP-Npas4. Densitometric scans of Npas4-WT in the absence and presence of MAP2K1-CA are shown.

(D) Immunoblots of Npas4 fragments expressed in COS7 cells with or without MAP2K1-CA after Laemmli's SDS-PAGE (upper panel) or Phos-tag SDS-PAGE (lower panel). Arrowheads indicate MAP2K1-dependent phosphorylated bands. Densitometric scans of Npas4 390–489 aas, Npas4 490–597 aas, or Npas4 598–701 aas in the absence and presence of MAP2K1-CA are shown on the bottom of the blot.

(E) The peak area values of dual-phosphorylated peptides obtained by SIM analysis were quantified. The data represent the mean ± SEM of three independent experiments. *$p < 0.05$; ****$p < 0.0001$.

(F) Phos-tag SDS-PAGE analysis of GFP-Npas4 390–489 aas, -WT, -T423A, -T427A, and -T423A/T427A. Densitometric comparison of the banding patterns between WT, T423A, T427A, and T423A/T427A in the presence of MAP2K1-CA is shown. Arrowheads indicate the positions of phosphorylated bands, which were absent in T423A/T427A mutant.

(G) Phos-tag SDS-PAGE analysis of GFP-Npas4 490–597 aas, -WT, -S577A, -S580A, and -S577A/S580A. Densitometric comparison of the banding patterns between WT, S577A, S580A, and S577A/S580A in the presence of MAP2K1-CA is shown. Arrowheads indicate the positions of phosphorylated bands, which were absent in S577A/S580A mutant.

(H) Phos-tag SDS-PAGE analysis of GFP-Npas4 598–700 aas, -WT, -T611A, -S615, and -T611A/S615A. Densitometric comparison of the banding patterns between WT, T611A, S615, and T611A/S615A in the presence of MAP2K1-CA is shown. Arrowheads indicate the positions of phosphorylated bands, which were absent in T611A/S615A mutant.

(I) Phos-tag SDS-PAGE analysis of GFP-Npas4-WT and -6A. Densitometric comparison of the banding patterns between WT and 6A in the absence and presence of MAP2K1-CA is shown. Arrowheads indicate the positions of phosphorylated bands, which were absent in 6A mutant.

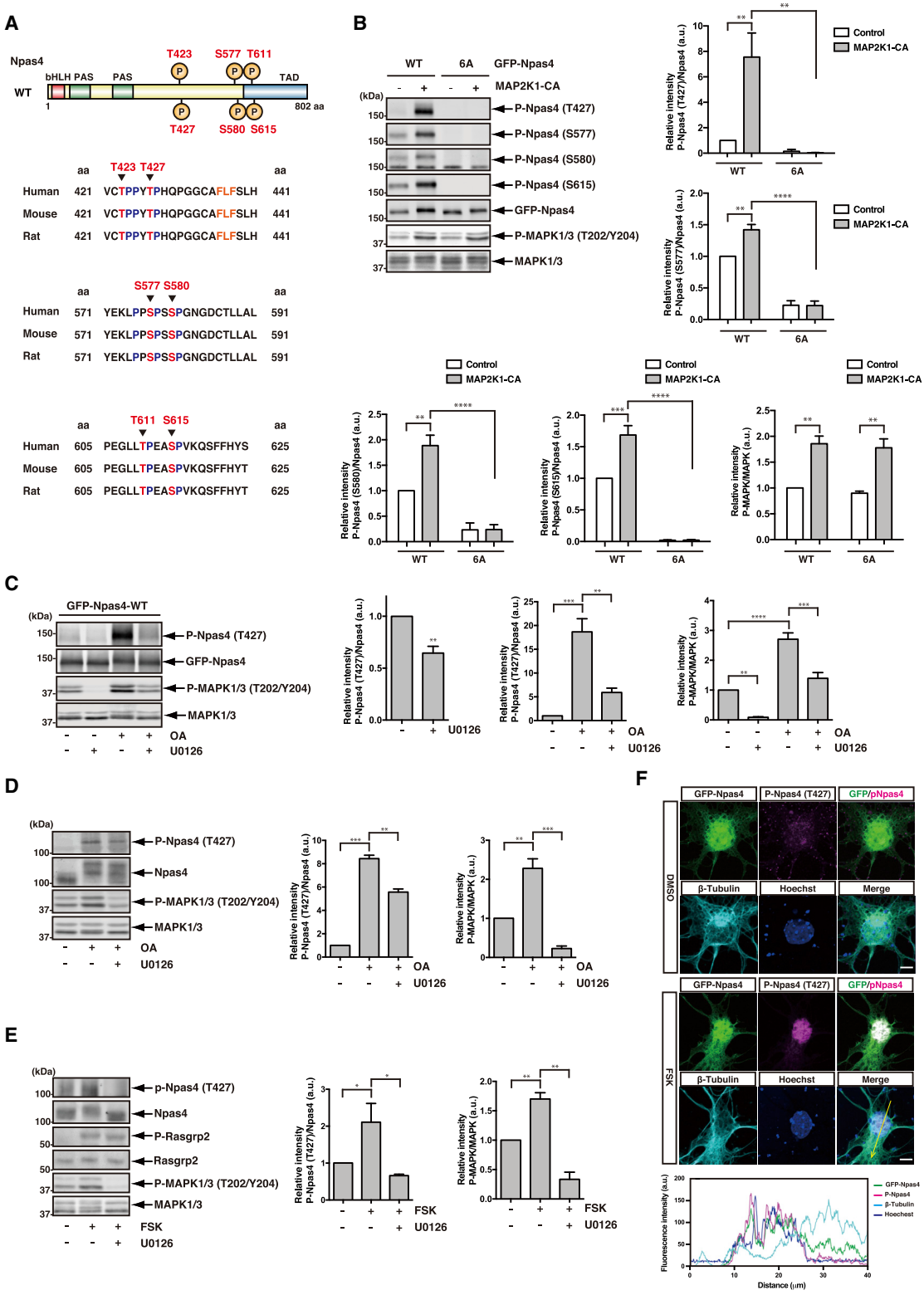

Figure 4. Phosphorylation of Npas4 by MAPK

(A) Schematic representation of MAPK dependent-phosphorylation sites in Npas4 and the alignment of phosphorylation sites in Npas4 homologs (human, mouse, and rat). Amino acids shown in red indicate the identified phosphorylation sites, amino acids shown in blue indicate proline residues that match the MAPK consensus motif, and amino acids shown in orange indicate a putative docking site. The numbers indicate amino acids.

(legend continued on next page)

cocaine treatment (Filip et al., 2006). To examine whether the MAPK-mediated phosphorylation of Npas4 modulates BDNF promoter activity, we performed a dual-reporter assay using the exon 1 BDNF promoter and found that the expression of GFP-Npas4-WT increased exon 1 BDNF promoter activity. This activity was further increased by MAP2K1-CA coexpression and by FSK treatment in cultured striatal neurons (Figures 5D and 5E). The expression of MAP2K1-CA or treatment of FSK did not significantly increase BDNF promoter activity without the expression of GFP-Npas4-WT (Figures 5D and 5E). We also found that, compared with Npas4-WT, Npas4-6A had reduced ability to activate exon 1 BDNF promoter and Npas4-6E enhanced exon 1 BDNF promoter activity (Figure 5F). These results suggest that the phosphorylation of Npas4 by MAPK increases BDNF promoter activity.

Npas4 and Its Phosphorylation in Accumbal D1R-MSNs Control Reward-Related Learning and Memory

To examine whether Npas4 is associated with reward-related learning and memory, we performed a cocaine-induced CPP test using Npas4 knockout (KO) mice. Before the CPP test, we checked whether Npas4 KO itself affects the D1R signaling pathway. Peritoneal injection of cocaine induced the phosphorylation of Rasgrp2 and MAPK1/3 in both WT and Npas4 KO mice (Figure S5A), indicating that the cocaine-induced activation of PKA and MAPK was normal in Npas4 KO mice. Cocaine injection induced place preference for the drug-paired side in WT mice, whereas the saline treatment did not result in place preference. The global knockout of Npas4 impaired cocaine-induced place preference (Figure S5B). This result is consistent with a recent study, which found that Npas4 knockout in the NAc impaired CPP (Taniguchi et al., 2017).

To further investigate whether Npas4 is required for reward learning and memory in D1R-MSNs or D2R-MSNs, we used Drd1a-Cre transgenic (tg) mice that express Cre-recombinase (Cre) specifically in D1R-MSNs (Gong et al., 2003) or adenosine A2a receptor (Adora2a)-Cre tg mice that express Cre specifically in D2R-MSNs (Gong et al., 2007). We established a system in which the dominant-negative form (DN) of Npas4 (Pruunsild et al., 2011; Yoshihara et al., 2014) was expressed in the NAc under the control of the D1R promoter or Adora2a promoter using adeno-associated virus (AAV)-mediated conditional transgene techniques (Figure 6A). The expression in the presence of Cre is achieved by Flex recombination of a transgene that changes the orientation of the coding sequence with respect to the promoter from the anti-sense to sense (Betley and Sternson, 2011; Figure 6A). We injected AAV-Flex-mCherry or AAV-Flex-mCherry-P2A-Npas4-DN into the NAc of Drd1a-Cre mice or Adora2a-Cre mice and performed the CPP test 2 to 3 weeks after viral injection (Figure 6B). Cocaine injection induced place preference to the drug-paired side in mCherry transfected mice, whereas the saline did not result in place preference. The rewarding effects of cocaine were markedly reduced in mice that expressed Npas4-DN in D1R-MSNs, but not in D2R-MSNs, in the NAc (Figure 6C). We also employed AAV-substance P (SP)-Cre and homozygous loxP-flanked (floxed) Npas4 mice (Npas4 fl/fl) to examine the specific functions of Npas4 in D1R-MSNs (Figure 6D). AAV-Flex-mCherry and AAV-SP-EGFP were coinjected with or without AAV-SP-Cre into the NAc of Npas4 fl/fl mice, and the CPP test was performed 2 to 3 weeks after viral injection (Figure 6B). The localized knockout of Npas4 in D1R-MSNs markedly decreased cocaine-induced place preference compared with the control AAV injection (Figure 6E). These results indicate that Npas4 in D1R-MSNs is required for reward-related learning and memory. To examine whether the phosphorylation of Npas4 regulates reward-related learning and memory, we coinjected AAV-Flex-mCherry-P2A-Npas4-WT or AAV-Flex-mCherry-P2A-Npas4-6A and AAV-SP-Cre into the NAc of Npas4 fl/fl mice (Figure 6E). The cocaine-induced CPP deficits in mice with local Npas4 knockout were restored by the expression of Npas4-WT, but not Npas4-6A (Figure 6E), suggesting that Npas4 phosphorylation in D1R-MSNs is important for reward-related learning and memory. Furthermore, to examine whether Npas4-6E rescued CPP when MAPK signaling was blocked, we coinfected AAV-SP-Cre and AAV-Flex-EGFP-P2A-MAP2K1-DN and/or AAV-Flex-mCherry-P2A-Npas4-WT or AAV-Flex-mCherry-P2A-Npas4-6E into the NAc (Figures S5C and S5D). The expression of MAP2K1-DN in D1R-MSNs significantly impaired cocaine-induced place preference. This defect could not be completely recovered by coexpression of Npas4-WT or 6E (Figures S5C and S5D), suggesting that additional MAPK substrates are also involved in reward-related learning and memory.

(B) The phosphorylation of GFP-Npas4 induced by MAP2K1-CA in COS7 cells. GFP-Npas4-WT or 6A was expressed in COS7 cells with or without the coexpression of MAP2K1-CA. The cell lysates were analyzed by immunoblotting with anti-pT427, anti-pS577, anti-pS580, anti-pS615, anti-GFP, anti-P-MAPK1/3, and anti-MAPK1/3 antibodies. The data represent the mean ± SEM of three independent experiments. $^{**}p < 0.01$; $^{***}p < 0.001$; $^{****}p < 0.0001$.

(C) The phosphorylation of GFP-Npas4 in COS7 cells under OA treatment. COS7 cells were transfected with GFP-Npas4-WT and were treated with DMSO or 10 μM U0126 for 30 min and then with or without 1 μM OA for 1 h. The cell lysates were analyzed by immunoblotting with anti-pT427, anti-GFP, anti-P-MAPK1/3, and anti-MAPK1/3 antibodies. The data represent the mean ± SEM of three independent experiments. $^{**}p < 0.01$; $^{***}p < 0.001$; $^{***}p < 0.0001$.

(D) The phosphorylation of endogenous Npas4 in cultured striatal neurons under OA treatment. Neurons were pretreated with 50 mM KCl for 1 h and were then treated with DMSO or 10 μM U0126 for 30 min and then with or without 1 μM OA for 1 h. The cell lysates were analyzed by immunoblotting with anti-pT427, anti-Npas4, anti-P-MAPK1/3, and anti-MAPK1/3 antibodies. The data represent the mean ± SEM of four independent experiments. $^{**}p < 0.01$; $^{***}p < 0.001$.

(E) The phosphorylation of endogenous Npas4 in cultured striatal neurons under FSK treatment. Striatal neurons were pretreated with 50 mM KCl for 1 h, treated with DMSO or 10 μM U0126 for 30 min, and then treated with or without 10 μM FSK for 30 min. The cell lysates were analyzed by immunoblotting with anti-pT427, anti-Npas4, anti-P-MAPK1/3, and anti-MAPK1/3 antibodies. $^{*}p < 0.05$; $^{**}p < 0.01$.

(F) The phosphorylation of Npas4 in the nuclei of cultured striatal neurons. Striatal neurons were transfected with GFP-Npas4-WT at 7 days *in vitro* (DIV) and treated with DMSO of 10 μM FSK for 30 min at 8 DIV. Neurons were immunostained with anti-GFP, anti-pT427, and anti-Tuj1 antibodies. Nuclei were visualized with Hoechst 33342. Scale bars, 5 μm. The graph plots the fluorescence intensities of GFP-Npas4 (green), phospho-Npas4 (T427) (magenta), Hoechst (blue), and β-tubulin (cyan) along the arrow.

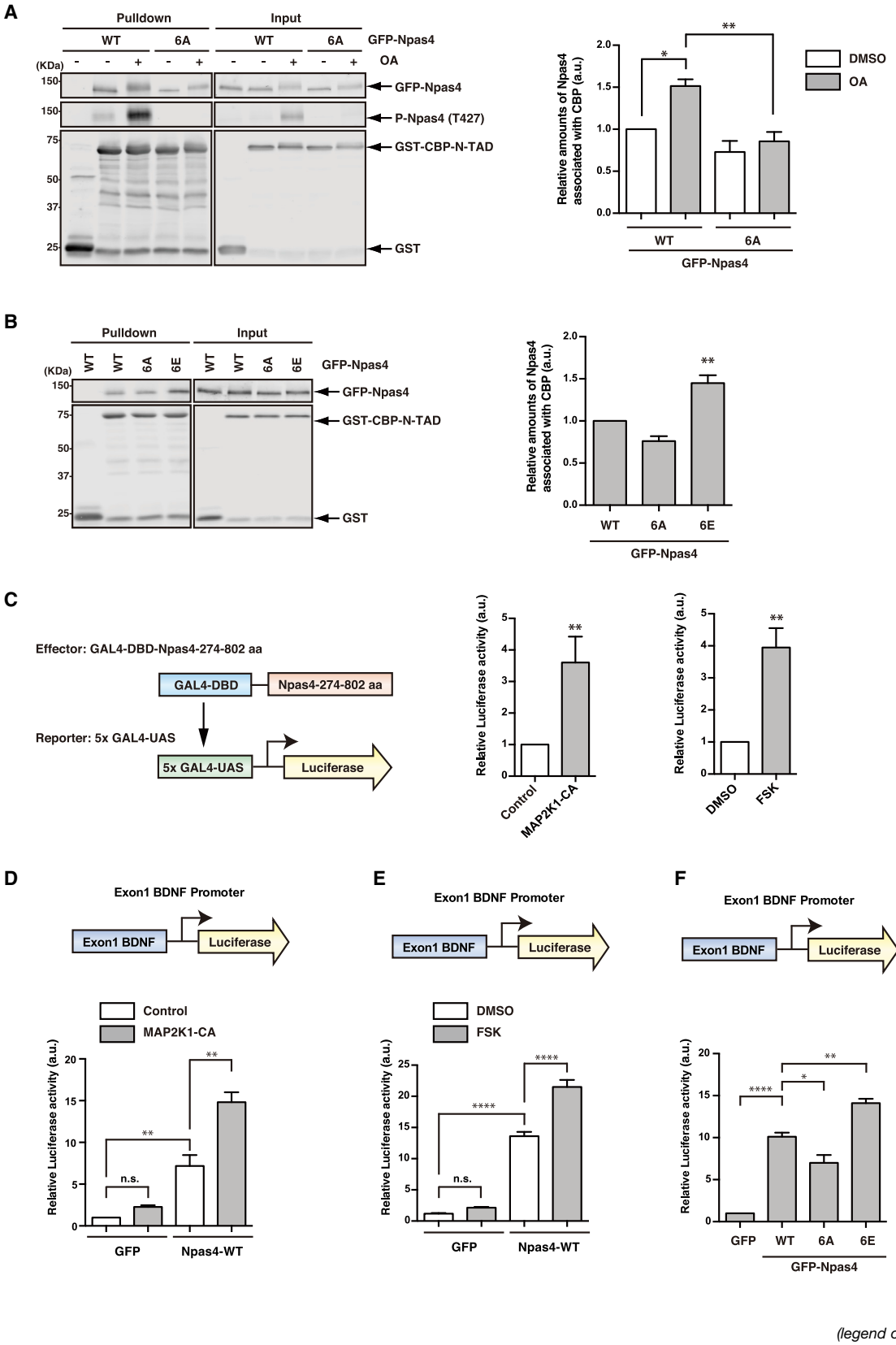

(legend on next page)

DISCUSSION

The Functional Significance of Npas4 Phosphorylation by MAPK

There is substantial evidence that Npas4 expression is regulated by activity-dependent Ca^{2+} signaling (Choy et al., 2015; Lin et al., 2008; Ramamoorthi et al., 2011) and PI3K-Akt signaling (Ooe et al., 2009; Speckmann et al., 2016). However, it is not well understood how Npas4 activity is regulated at the posttranslational level. In the present study, we found that MAPK directly phosphorylated Npas4 in an *in vitro* kinase assay (Figure 3B) and that MAP2K1-CA induced a clear band shift of Npas4 in Phos-tag SDS-PAGE (Figure 3C). These observations, together with the previous finding that MAP2K inhibitor treatment prevents a band shift of Npas4 in Laemmli's SDS-PAGE (Ooe et al., 2009; Speckmann et al., 2016), indicate that MAPK directly phosphorylates Npas4. Furthermore, with LC-MS/MS and phos-tag SDS-PAGE analysis, we identified the sites of Npas4 phosphorylation by MAPK as T423, T427, S577, S580, T611, and S615 (Figures 3D–3H). These multiple phosphorylation sites are located in the middle region and C-terminal region of the TAD domain, not in the N-terminal region of the DNA-binding domain, suggesting that the MAPK-dependent phosphorylation of Npas4 affects transcriptional activity through protein interaction, but not DNA binding. We found that Npas4 274–802 aas interacted with the N-TAD domain of CBP, which was increased in a MAPK activity-dependent manner (Figures 2E and 2F). Consistently, MAPK signal activation through the expression of MAP2K1-CA or FSK treatment enhanced the transcriptional activity of Npas4 (Figures 5C–5E). Furthermore, the Npas4-6A mutant showed reduced transcriptional activity and the Npas4-6E mutant showed enhanced transcriptional activity (Figure 5F). Taken together, these observations suggest that the phosphorylation of Npas4 by MAPK enhances the transcriptional activity of Npas4 through CBP binding.

Role of Npas4 in Reward-Related Learning and Memory in D1R-MSNs

It has been reported that Npas4 in the hippocampal CA3 region is required for normal social interaction and contextual fear memory formation (Coutellier et al., 2012; Ramamoorthi et al., 2011). However, the functional role of Npas4 in the NAc and reward-related behaviors is not well understood. A recent study has shown that Npas4 knockout in the NAc impairs CPP (Taniguchi et al., 2017). However, virus-based approaches using nonspecific Cre inactivate all neurons in the injection area, and it remains unclear which neuronal population is responsible for Npas4-dependent reward effects. Indeed, we previously found that the selective expression of MAP2K1-CA in D1R-MSNs significantly potentiated methamphetamine-induced conditioned place preference, whereas the expression of MAP2K1-CA in D2R-MSNs in the NAc did not (Bin Saifullah et al., 2018). In the present study, we found that Npas4 was mainly expressed in D1R-MSNs after CPP training (Figure 1F). To analyze D1R-specific Npas4 function, Npas4-DN was expressed in the NAc under the control of the D1R or Adora2a promoter using AAV-mediated conditional transgenic techniques (Figure 6A). The rewarding effects of cocaine were markedly potentiated in mice that expressed Npas4-DN in D1R-MSNs, but not in D2R-MSNs, of the NAc (Figure 6C). We also administered AAV-SP-Cre into the NAc of homozygous floxed Npas4 mice (Npas4 fl/fl) (Figure 6D). The D1R-specific knockout of Npas4 notably diminished cocaine-induced CPP (Figure 6E). This deficit in mice with local knockout of Npas4 was restored by the expression of Npas4-WT, but not Npas4-6A (Figure 6E), indicating that Npas4 phosphorylation in D1R-MSNs is important for reward-related learning and memory.

Target Genes of Npas4 in Reward-Related Learning and Memory

In the present study, we found that the expression of Npas4 increased exon 1 BDNF promoter activity and that the phosphorylation of Npas4 enhanced its activity (Figures 5D–5F). Npas4 and its phosphorylation were required for cocaine-induced CPP (Figure 6C and 6E). Our findings raise the possibility that Npas4 and its phosphorylation regulate BDNF expression to form long-term reward-related memory. It has been reported that the expression of *Bdnf* is upregulated in the NAc of animals conditioned in a CPP task (Tian et al., 2016) and that the expression of lentivirus-BDNF and TrkB enhanced cocaine-induced CPP (Bahi et al., 2008). In addition to BDNF, Npas4 can regulate the expression of several genes that are important for neuronal survival and synaptic plasticity, such as *c-Fos*, *Zif268*, *Arc/Arg3.1*, and *Homer1a* (Lin et al., 2008; Pruunsild et al., 2011;

Figure 5. Effects of the Phosphorylation of Npas4 on Its Interaction with CBP; Transcriptional Regulation by Npas4 Phosphorylation

(A) COS7 cells were cotransfected with GST or GST-CBP-N-TAD and GFP-Npas4-WT or GFP-Npas4-6A and then treated with or without OA for 1 h. Extracts of COS7 cells were incubated with glutathione beads. The bound proteins were subjected to immunoblot analysis using an anti-GFP or anti-GST antibody. The data represent the mean ± SEM of three independent experiments. *$p < 0.05$; **$p < 0.01$.

(B) COS7 cells were cotransfected with GST or GST-CBP-N-TAD and GFP-Npas4-WT, -6A, or -6E. Extracts of COS7 cells were incubated with glutathione beads. The bound proteins were subjected to immunoblot analysis using an anti-GFP or anti-GST antibody. The data represent the mean ± SEM of three independent experiments. **$p < 0.01$.

(C) The transcriptional activity of Gal4-DBD-Npas4-274–802 aas was enhanced by MAP2K1-CA coexpression, as well as FSK treatment. The data represent the mean ± SEM. **$p < 0.01$.

(D) Effect of Npas4 on transcriptional activity of the exon 1 BDNF promoter with or without the coexpression of MAP2K1-CA. The data represent the mean ± SEM of four independent experiments. **$p < 0.01$.

(E) Effect of Npas4 on transcriptional activity of the exon 1 BDNF promoter with or without FSK treatment for 4 h. The data represent the mean ± SEM of four independent experiments. ****$p < 0.0001$.

(F) Effect of Npas4 mutant on transcriptional activity of the exon 1 BDNF promoter. The data represent the mean ± SEM of four independent experiments. *$p < 0.05$; **$p < 0.01$; ****$p < 0.0001$.

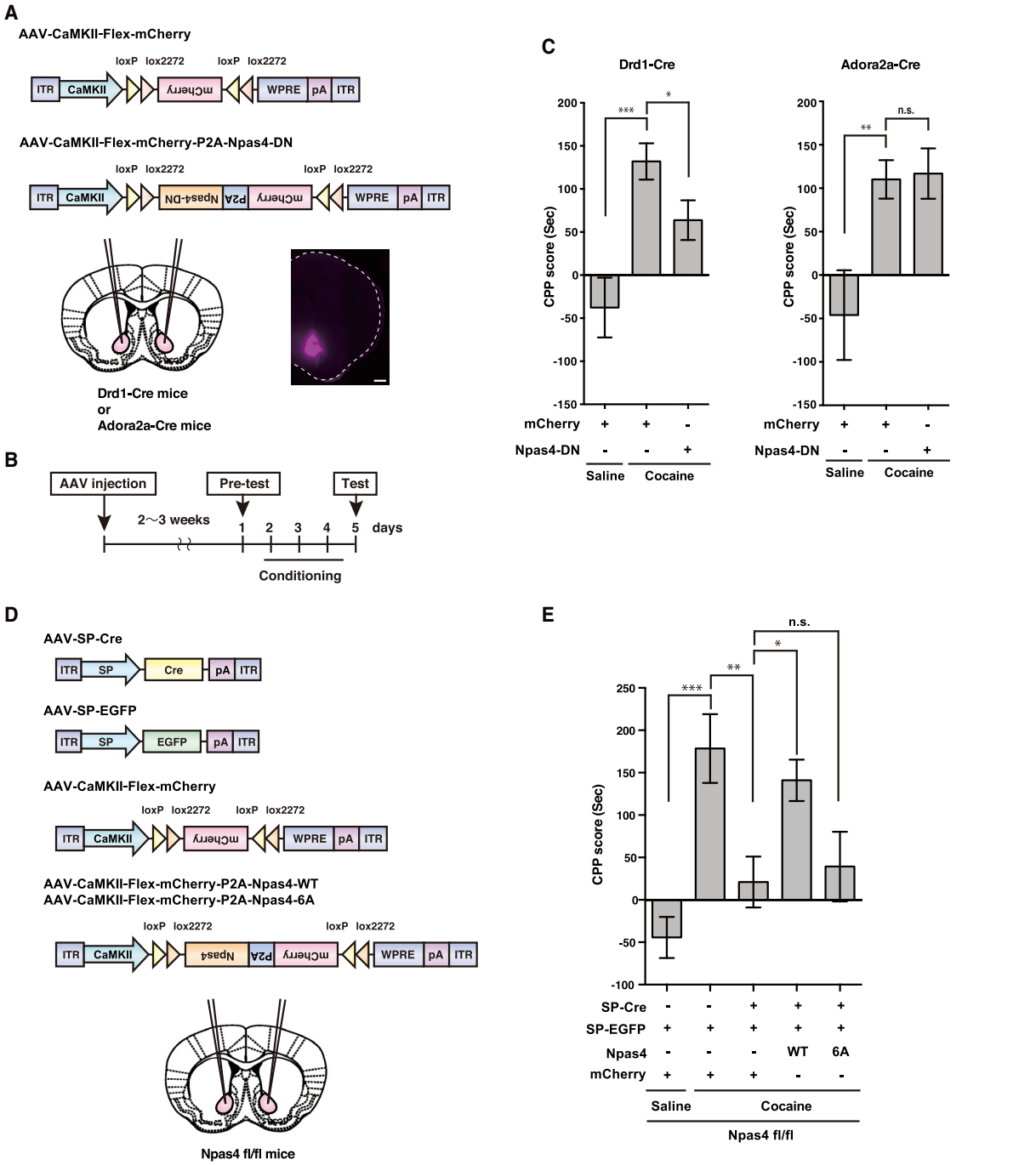

Figure 6. Npas4 and Its Phosphorylation in Accumbal D1R-MSNs Control Reward-Related Learning and Memory

(A) Schematic of AAV-mediated conditional Npas4-DN expression in accumbal D1R-MSNs and D2R-MSNs. The diagram shows the AAV constructs and stereotaxic injection of AAV into the NAc of Drd1-Cre tg or Adora2a-Cre tg mice. Representative coronal brain slices show the expression of mCherry 2 weeks after AAV injection into the NAc (bottom panel). The scale bar represents 300 μm.

(B) Experimental schedule.

(C) Effect of Npas4-DN on cocaine-induced place preference in D1R-MSNs and in D2R-MSNs. The data represent the mean ± SEM. *$p < 0.05$; **$p < 0.01$; ***$p < 0.001$ (mCherry, saline n = 17; mCherry, cocaine n = 19; Npas4-DN, cocaine n = 22; in Drd1-Cre; mCherry, saline n = 5; mCherry, cocaine n = 5; Npas4-DN, cocaine n = 10; in Adora2a-Cre).

(D) Schematic of AAV-mediated conditional Npas4 knockout in accumbal D1R-MSNs. The diagram shows the AAV constructs and stereotaxic injection of AAV into the NAc of Npas4 fl/fl mice.

(legend continued on next page)

Shan et al., 2018; Spiegel et al., 2014; Yoshihara et al., 2014). It has been reported that cocaine injection predominantly induces the expression of *c-Fos* and *Zif268* in D1R-expressing MSNs (Bertran-Gonzalez et al., 2008) and increases *Arc/Arg3.1* mRNA levels in the striatum (Caffino et al., 2011). Cocaine injection has been shown to induce Homer1a protein expression in the striatum, and this increase was blocked by a D1R antagonist, but not a D2R antagonist (Patil et al., 2007). A recent study has shown that Homer1a deletion reduces cocaine-induced behavioral sensitization but has no effect on cocaine-induced CPP (Datko et al., 2017). Exploring the role of Npas4 target genes in reward-related learning and memory will be an important future direction.

Roles of CBP-Interacting Proteins

CBP is a multipurpose transcriptional coactivator that participates in a diverse array of basic cellular functions, including DNA repair, cell growth, differentiation, apoptosis, synaptic plasticity, and memory. These functions of CBP are regulated by protein-protein interactions between CBP and other transcriptional regulators. Such interactions regulate gene activation and subsequent cell functions. In this study, a proteomic screening of mouse striatal tissue using the N-terminal transactivation domain of CBP as bait identified several CBP-interacting partners, including CREB, Histone H3, FosB, ΔFosB, Jun, Npas4, Mkl2, Matrin-3, and Pur-alpha (Figures 1A–1C). CREB and ΔFosB are well-known CBP-interacting proteins that are implicated in reward-related behavior (Carlezon et al., 1998; Kelz et al., 1999; Nestler et al., 1999). Here, we focused specifically on Npas4 and revealed that MAPK regulated the CBP-Npas4 interaction to enhance reward-related memory. Mkl2 and matrin-3 were identified as other potential CBP-interacting partners. Mkl1 (MAL/MRTF-A/BSAC) and Mkl2 (MRTF-B/MAL16) are coactivators that interact with serum response factor (SRF) and regulate SRF-dependent gene expression (Kalita et al., 2012). Mkl1 and Mkl2 are involved in the reorganization of dendritic spines and the complexity of dendrites (Ishikawa et al., 2010). The deletion of SRF from the NAc decreases animals' sensitivity to the rewarding effects of cocaine (Vialou et al., 2012). It is possible that the interactions among Mkl2, SRF, and CBP cooperate to regulate reward-related memory formation. Matrin-3 is an inner nuclear matrix protein with two zinc finger domains and two RNA recognition motifs (RRMs) (Salton et al., 2011). The nuclear matrix participates in DNA replication, transcription, RNA processing, and chromatin organization. Matrin-3 is reported to be phosphorylated by PKA following the activation of NMDA receptors, a process that leads to its degradation (Giordano et al., 2005). This PKA-mediated phosphorylation of Matrin-3 and the modulation of nuclear matrix function could be involved in long-term potentiation (Giordano et al., 2005). Future research on these CBP-interacting proteins could identify novel mechanisms involved in reward-related learning and memory.

STAR★METHODS

Detailed methods are provided in the online version of this paper and include the following:

- KEY RESOURCES TABLE
- LEAD CONTACT AND MATERIALS AVAILABILITY
- EXPERIMENTAL MODEL AND SUBJECT DETAILS
  - Animals
  - Cell Lines
  - Primary Cell Cultures
- METHOD DETAILS
  - Materials
  - Plasmid Constructs
  - Laemmli's SDS-PAGE, Phos-tag SDS-PAGE, and Immunoblotting
  - *In Vitro* Phosphorylation Assay
  - GST Pulldown Assay
  - Mass Spectrometry
  - Data Analysis for Mass Spectrometry
  - Immunofluorescence Analysis
  - Dual-Luciferase Reporter Assay
  - AAV Preparation and Injection
  - Behavioral Analysis
- QUANTIFICATION AND STATISTICAL ANALYSIS
- DATA AND CODE AVAILABILITY

SUPPLEMENTAL INFORMATION

Supplemental Information can be found online at https://doi.org/10.1016/j.celrep.2019.10.116.

ACKNOWLEDGMENTS

We thank Dr. M.E. Greenberg for providing Npas4 KO/flox mice and Dr. K. Kobayashi for providing Drd1-mVenus/Drd2-mVenus transgenic mice. We are grateful to T. Watanabe, D. Tsuboi, T. Nishioka, Y. Yamahashi, X. Zhang, E. Hossen, M. Taguchi, K. Hada, and other Kaibuchi and Yamada lab members for helpful discussions and preparation of some materials; F. Ishidate for help with image acquisition; K. Taki for help with MS data acquisition; and T. Ishii for secretarial assistance. We also thank the Division for Research on Laboratory Animals and Medical Research Engineering of Nagoya University Graduate School of Medicine. This work was supported by the following funding sources: "Bioinformatics for Brain Sciences" performed under the SRPBS from MEXT and AMED; AMED grant numbers JP18dm0207005, JP19dm0207075, and JP19dm0307025; JSPS KAKENHI grant numbers JP16K18393, JP17H01380, JP17J09461, JP17K07383, JP17H02220, JP17K19483, JP18K14816, and JP18K14849; MEXT KAKENHI grant numbers JP17H05561 and JP19H05209; Uehara Memorial Foundation; and Takeda Science Foundation.

AUTHOR CONTRIBUTIONS

Conceptualization, Y.F. and K. Kaibuchi; Methodology, T.T., Y.Y., K. Kuroda, T.N., and K.Y.; Formal Analysis, Y.F., A.A., and R.E.; Investigation, Y.F., A.A., R.E., Y.X., K.S., S.K., R.U.A., and M.A.; Resources, S.W., M.W., Y.Y.,

(E) AAV-mediated knockout of Npas4 in D1R-MSNs attenuated cocaine-induced CPP, and cocaine-induced CPP was restored by the expression of Npas4-WT, but not Npas4-6A. The data represent the mean ± SEM. *$p < 0.05$; **$p < 0.01$; ***$p < 0.001$. In the control group, AAV-SP-EGFP and AAV-Flex-mCherry were injected into the NAc (SP-Cre(−)/mCherry/saline n = 11; SP-Cre(−)/mCherry/cocaine n = 14; SP-Cre(+)/mCherry/cocaine n = 11; SP-Cre(+)/Npas4-WT/cocaine n = 9; SP-Cre(+)/Npas4-6A/cocaine n = 10 in Npas4 fl/fl).

K. Kuroda, T.N., and K.Y.; Data Curation, Y.F.; Writing, Y.F., A.A., and K. Kaibuchi.

DECLARATION OF INTERESTS

The authors declare no competing interests.

Received: June 4, 2018
Revised: September 2, 2019
Accepted: October 28, 2019
Published: December 3, 2019

REFERENCES

Amano, M., Hamaguchi, T., Shohag, M.H., Kozawa, K., Kato, K., Zhang, X., Yura, Y., Matsuura, Y., Kataoka, C., Nishioka, T., and Kaibuchi, K. (2015). Kinase-interacting substrate screening is a novel method to identify kinase substrates. J. Cell Biol. *209*, 895–912.

Bahi, A., Boyer, F., Chandrasekar, V., and Dreyer, J.L. (2008). Role of accumbens BDNF and TrkB in cocaine-induced psychomotor sensitization, conditioned-place preference, and reinstatement in rats. Psychopharmacology (Berl.) *199*, 169–182.

Barrett, R.M., and Wood, M.A. (2008). Beyond transcription factors: the role of chromatin modifying enzymes in regulating transcription required for memory. Learn. Mem. *15*, 460–467.

Bekinschtein, P., Cammarota, M., Katche, C., Slipczuk, L., Rossato, J.I., Goldin, A., Izquierdo, I., and Medina, J.H. (2008). BDNF is essential to promote persistence of long-term memory storage. Proc. Natl. Acad. Sci. USA *105*, 2711–2716.

Bertran-Gonzalez, J., Bosch, C., Maroteaux, M., Matamales, M., Hervé, D., Valjent, E., and Girault, J.A. (2008). Opposing patterns of signaling activation in dopamine D1 and D2 receptor-expressing striatal neurons in response to cocaine and haloperidol. J. Neurosci. *28*, 5671–5685.

Betley, J.N., and Sternson, S.M. (2011). Adeno-associated viral vectors for mapping, monitoring, and manipulating neural circuits. Hum. Gene Ther. *22*, 669–677.

Bin Saifullah, M.A., Nagai, T., Kuroda, K., Wulaer, B., Nabeshima, T., Kaibuchi, K., and Yamada, K. (2018). Cell type-specific activation of mitogen-activated protein kinase in D1 receptor-expressing neurons of the nucleus accumbens potentiates stimulus-reward learning in mice. Sci. Rep. *8*, 14413.

Bloodgood, B.L., Sharma, N., Browne, H.A., Trepman, A.Z., and Greenberg, M.E. (2013). The activity-dependent transcription factor NPAS4 regulates domain-specific inhibition. Nature *503*, 121–125.

Caffino, L., Racagni, G., and Fumagalli, F. (2011). Stress and cocaine interact to modulate Arc/Arg3.1 expression in rat brain. Psychopharmacology (Berl.) *218*, 241–248.

Carlezon, W.A., Jr., Thome, J., Olson, V.G., Lane-Ladd, S.B., Brodkin, E.S., Hiroi, N., Duman, R.S., Neve, R.L., and Nestler, E.J. (1998). Regulation of cocaine reward by CREB. Science *282*, 2272–2275.

Carlsson, A. (2001). A paradigm shift in brain research. Science *294*, 1021–1024.

Choe, E.S., and McGinty, J.F. (2000). N-Methyl-D-aspartate receptors and p38 mitogen-activated protein kinase are required for cAMP-dependent cyclase response element binding protein and Elk-1 phosphorylation in the striatum. Neuroscience *101*, 607–617.

Choe, E.S., and McGinty, J.F. (2001). Cyclic AMP and mitogen-activated protein kinases are required for glutamate-dependent cyclic AMP response element binding protein and Elk-1 phosphorylation in the dorsal striatum in vivo. J. Neurochem. *76*, 401–412.

Choy, F.C., Klarić, T.S., Koblar, S.A., and Lewis, M.D. (2015). The role of the neuroprotective factor Npas4 in cerebral ischemia. Int. J. Mol. Sci. *16*, 29011–29028.

Chrivia, J.C., Kwok, R.P., Lamb, N., Hagiwara, M., Montminy, M.R., and Goodman, R.H. (1993). Phosphorylated CREB binds specifically to the nuclear protein CBP. Nature *365*, 855–859.

Coutellier, L., Beraki, S., Ardestani, P.M., Saw, N.L., and Shamloo, M. (2012). Npas4: a neuronal transcription factor with a key role in social and cognitive functions relevant to developmental disorders. PLoS ONE *7*, e46604.

Cowan, C.W., Shao, Y.R., Sahin, M., Shamah, S.M., Lin, M.Z., Greer, P.L., Gao, S., Griffith, E.C., Brugge, J.S., and Greenberg, M.E. (2005). Vav family GEFs link activated Ephs to endocytosis and axon guidance. Neuron *46*, 205–217.

Dash, P.K., Karl, K.A., Colicos, M.A., Prywes, R., and Kandel, E.R. (1991). cAMP response element-binding protein is activated by Ca2+/calmodulin- as well as cAMP-dependent protein kinase. Proc. Natl. Acad. Sci. USA *88*, 5061–5065.

Datko, M.C., Hu, J.H., Williams, M., Reyes, C.M., Lominac, K.D., von Jonquieres, G., Klugmann, M., Worley, P.F., and Szumlinski, K.K. (2017). Behavioral and neurochemical phenotyping of mice incapable of Homer1a induction. Front. Behav. Neurosci. *11*, 208.

Filip, M., Faron-Górecka, A., Kuśmider, M., Gołda, A., Frankowska, M., and Dziedzicka-Wasylewska, M. (2006). Alterations in BDNF and trkB mRNAs following acute or sensitizing cocaine treatments and withdrawal. Brain Res. *1071*, 218–225.

Funahashi, Y., Namba, T., Fujisue, S., Itoh, N., Nakamuta, S., Kato, K., Shimada, A., Xu, C., Shan, W., Nishioka, T., and Kaibuchi, K. (2013). ERK2-mediated phosphorylation of Par3 regulates neuronal polarization. J. Neurosci. *33*, 13270–13285.

Giordano, G., Sánchez-Pérez, A.M., Montoliu, C., Berezney, R., Malyavantham, K., Costa, L.G., Calvete, J.J., and Felipo, V. (2005). Activation of NMDA receptors induces protein kinase A-mediated phosphorylation and degradation of matrin 3. Blocking these effects prevents NMDA-induced neuronal death. J. Neurochem. *94*, 808–818.

Girault, J.A., and Greengard, P. (2004). The neurobiology of dopamine signaling. Arch. Neurol. *61*, 641–644.

Gong, S., Zheng, C., Doughty, M.L., Losos, K., Didkovsky, N., Schambra, U.B., Nowak, N.J., Joyner, A., Leblanc, G., Hatten, M.E., and Heintz, N. (2003). A gene expression atlas of the central nervous system based on bacterial artificial chromosomes. Nature *425*, 917–925.

Gong, S., Doughty, M., Harbaugh, C.R., Cummins, A., Hatten, M.E., Heintz, N., and Gerfen, C.R. (2007). Targeting Cre recombinase to specific neuron populations with bacterial artificial chromosome constructs. J. Neurosci. *27*, 9817–9823.

Hervé, D., Lévi-Strauss, M., Marey-Semper, I., Verney, C., Tassin, J.P., Glowinski, J., and Girault, J.A. (1993). G(olf) and Gs in rat basal ganglia: possible involvement of G(olf) in the coupling of dopamine D1 receptor with adenylyl cyclase. J. Neurosci. *13*, 2237–2248.

Hikida, T., Kimura, K., Wada, N., Funabiki, K., and Nakanishi, S. (2010). Distinct roles of synaptic transmission in direct and indirect striatal pathways to reward and aversive behavior. Neuron *66*, 896–907.

Huang da, W., Sherman, B.T., and Lempicki, R.A. (2009a). Bioinformatics enrichment tools: paths toward the comprehensive functional analysis of large gene lists. Nucleic Acids Res. *37*, 1–13.

Huang da, W., Sherman, B.T., and Lempicki, R.A. (2009b). Systematic and integrative analysis of large gene lists using DAVID bioinformatics resources. Nat. Protoc. *4*, 44–57.

Hyman, S.E., and Malenka, R.C. (2001). Addiction and the brain: the neurobiology of compulsion and its persistence. Nat. Rev. Neurosci. *2*, 695–703.

Hyman, S.E., Malenka, R.C., and Nestler, E.J. (2006). Neural mechanisms of addiction: the role of reward-related learning and memory. Annu. Rev. Neurosci. *29*, 565–598.

Ishikawa, M., Nishijima, N., Shiota, J., Sakagami, H., Tsuchida, K., Mizukoshi, M., Fukuchi, M., Tsuda, M., and Tabuchi, A. (2010). Involvement of the serum response factor coactivator megakaryoblastic leukemia (MKL) in the activin-regulated dendritic complexity of rat cortical neurons. J. Biol. Chem. *285*, 32734–32743.

Iversen, S.D., and Iversen, L.L. (2007). Dopamine: 50 years in perspective. Trends Neurosci. *30*, 188–193.

Kalita, K., Kuzniewska, B., and Kaczmarek, L. (2012). MKLs: co-factors of serum response factor (SRF) in neuronal responses. Int. J. Biochem. Cell Biol. *44*, 1444–1447.

Karamouzis, M.V., Konstantinopoulos, P.A., and Papavassiliou, A.G. (2007). Roles of CREB-binding protein (CBP)/p300 in respiratory epithelium tumorigenesis. Cell Res. *17*, 324–332.

Kelz, M.B., Chen, J., Carlezon, W.A., Jr., Whisler, K., Gilden, L., Beckmann, A.M., Steffen, C., Zhang, Y.J., Marotti, L., Self, D.W., et al. (1999). Expression of the transcription factor deltaFosB in the brain controls sensitivity to cocaine. Nature *401*, 272–276.

Kinoshita, E., Kinoshita-Kikuta, E., Takiyama, K., and Koike, T. (2006). Phosphate-binding tag, a new tool to visualize phosphorylated proteins. Mol. Cell. Proteomics *5*, 749–757.

Koob, G.F., and Volkow, N.D. (2010). Neurocircuitry of addiction. Neuropsychopharmacology *35*, 217–238.

Leong, W.K., Klaric, T.S., Lin, Y., Lewis, M.D., and Koblar, S.A. (2013). Upregulation of the neuronal Per-Arnt-Sim domain protein 4 (Npas4) in the rat corticolimbic system following focal cerebral ischemia. Eur. J. Neurosci. *37*, 1875–1884.

Lin, Y., Bloodgood, B.L., Hauser, J.L., Lapan, A.D., Koon, A.C., Kim, T.K., Hu, L.S., Malik, A.N., and Greenberg, M.E. (2008). Activity-dependent regulation of inhibitory synapse development by Npas4. Nature *455*, 1198–1204.

Malvaez, M., Mhillaj, E., Matheos, D.P., Palmery, M., and Wood, M.A. (2011). CBP in the nucleus accumbens regulates cocaine-induced histone acetylation and is critical for cocaine-associated behaviors. J. Neurosci. *31*, 16941–16948.

McClung, C.A., and Nestler, E.J. (2008). Neuroplasticity mediated by altered gene expression. Neuropsychopharmacology *33*, 3–17.

Montminy, M.R., Gonzalez, G.A., and Yamamoto, K.K. (1990). Regulation of cAMP-inducible genes by CREB. Trends Neurosci. *13*, 184–188.

Nagai, T., Nakamuta, S., Kuroda, K., Nakauchi, S., Nishioka, T., Takano, T., Zhang, X., Tsuboi, D., Funahashi, Y., Nakano, T., et al. (2016). Phosphoproteomics of the dopamine pathway enables discovery of Rap1 activation as a reward signal in vivo. Neuron *89*, 550–565.

Nestler, E.J. (2001). Molecular basis of long-term plasticity underlying addiction. Nat. Rev. Neurosci. *2*, 119–128.

Nestler, E.J., Kelz, M.B., and Chen, J. (1999). DeltaFosB: a molecular mediator of long-term neural and behavioral plasticity. Brain Res. *835*, 10–17.

Ooe, N., Saito, K., Mikami, N., Nakatuka, I., and Kaneko, H. (2004). Identification of a novel basic helix-loop-helix-PAS factor, NXF, reveals a Sim2 competitive, positive regulatory role in dendritic-cytoskeleton modulator drebrin gene expression. Mol. Cell. Biol. *24*, 608–616.

Ooe, N., Kobayashi, K., Motonaga, K., Saito, K., and Kaneko, H. (2009). Dynamic regulation of bHLH-PAS-type transcription factor NXF gene expression and neurotrophin dependent induction of the transcriptional control activity. Biochem. Biophys. Res. Commun. *378*, 761–765.

Parker, D., Ferreri, K., Nakajima, T., LaMorte, V.J., Evans, R., Koerber, S.C., Hoeger, C., and Montminy, M.R. (1996). Phosphorylation of CREB at Ser-133 induces complex formation with CREB-binding protein via a direct mechanism. Mol. Cell. Biol. *16*, 694–703.

Patil, S.T., Zhang, L., Martenyi, F., Lowe, S.L., Jackson, K.A., Andreev, B.V., Avedisova, A.S., Bardenstein, L.M., Gurovich, I.Y., Morozova, M.A., et al. (2007). Activation of mGlu2/3 receptors as a new approach to treat schizophrenia: a randomized Phase 2 clinical trial. Nat. Med. *13*, 1102–1107.

Phillips, A.G., Vacca, G., and Ahn, S. (2008). A top-down perspective on dopamine, motivation and memory. Pharmacol. Biochem. Behav. *90*, 236–249.

Pruunsild, P., Sepp, M., Orav, E., Koppel, I., and Timmusk, T. (2011). Identification of cis-elements and transcription factors regulating neuronal activity-dependent transcription of human BDNF gene. J. Neurosci. *31*, 3295–3308.

Ramamoorthi, K., Fropf, R., Belfort, G.M., Fitzmaurice, H.L., McKinney, R.M., Neve, R.L., Otto, T., and Lin, Y. (2011). Npas4 regulates a transcriptional program in CA3 required for contextual memory formation. Science *334*, 1669–1675.

Renthal, W., and Nestler, E.J. (2008). Epigenetic mechanisms in drug addiction. Trends Mol. Med. *14*, 341–350.

Robinson, T.E., and Kolb, B. (1999). Alterations in the morphology of dendrites and dendritic spines in the nucleus accumbens and prefrontal cortex following repeated treatment with amphetamine or cocaine. Eur. J. Neurosci. *11*, 1598–1604.

Rogge, G.A., and Wood, M.A. (2013). The role of histone acetylation in cocaine-induced neural plasticity and behavior. Neuropsychopharmacology *38*, 94–110.

Salton, M., Elkon, R., Borodina, T., Davydov, A., Yaspo, M.L., Halperin, E., and Shiloh, Y. (2011). Matrin 3 binds and stabilizes mRNA. PLoS ONE *6*, e23882.

Shan, W., Nagai, T., Tanaka, M., Itoh, N., Furukawa-Hibi, Y., Nabeshima, T., Sokabe, M., and Yamada, K. (2018). Neuronal PAS domain protein 4 (Npas4) controls neuronal homeostasis in pentylenetetrazole-induced epilepsy through the induction of Homer1a. J. Neurochem *145*, 19–33.

Sheng, M., Thompson, M.A., and Greenberg, M.E. (1991). CREB: a Ca(2+)-regulated transcription factor phosphorylated by calmodulin-dependent kinases. Science *252*, 1427–1430.

Smith, R.J., Lobo, M.K., Spencer, S., and Kalivas, P.W. (2013). Cocaine-induced adaptations in D1 and D2 accumbens projection neurons (a dichotomy not necessarily synonymous with direct and indirect pathways). Curr. Opin. Neurobiol. *23*, 546–552.

Sooksawate, T., Isa, K., Matsui, R., Kato, S., Kinoshita, M., Kobayashi, K., Watanabe, D., Kobayashi, K., and Isa, T. (2013). Viral vector-mediated selective and reversible blockade of the pathway for visual orienting in mice. Front. Neural Circuits *7*, 162.

Speckmann, T., Sabatini, P.V., Nian, C., Smith, R.G., and Lynn, F.C. (2016). Npas4 transcription factor expression is regulated by calcium signaling pathways and prevents tacrolimus-induced cytotoxicity in pancreatic beta cells. J. Biol. Chem. *291*, 2682–2695.

Spiegel, I., Mardinly, A.R., Gabel, H.W., Bazinet, J.E., Couch, C.H., Tzeng, C.P., Harmin, D.A., and Greenberg, M.E. (2014). Npas4 regulates excitatory-inhibitory balance within neural circuits through cell-type-specific gene programs. Cell *157*, 1216–1229.

Stoof, J.C., and Kebabian, J.W. (1984). Two dopamine receptors: biochemistry, physiology and pharmacology. Life Sci. *35*, 2281–2296.

Swanson, J.M., Kinsbourne, M., Nigg, J., Lanphear, B., Stefanatos, G.A., Volkow, N., Taylor, E., Casey, B.J., Castellanos, F.X., and Wadhwa, P.D. (2007). Etiologic subtypes of attention-deficit/hyperactivity disorder: brain imaging, molecular genetic and environmental factors and the dopamine hypothesis. Neuropsychol. Rev. *17*, 39–59.

Taniguchi, M., Carreira, M.B., Cooper, Y.A., Bobadilla, A.C., Heinsbroek, J.A., Koike, N., Larson, E.B., Balmuth, E.A., Hughes, B.W., Penrod, R.D., et al. (2017). HDAC5 and its target gene, Npas4, function in the nucleus accumbens to regulate cocaine-conditioned behaviors. Neuron *96*, 130–144.e6.

Tian, W., Wang, J., Zhang, K., Teng, H., Li, C., Szyf, M., Sun, Z.S., and Zhao, M. (2016). Demethylation of c-MYB binding site mediates upregulation of Bdnf IV in cocaine-conditioned place preference. Sci. Rep. *6*, 22087.

Tsai, L.N., Ku, T.K., Salib, N.K., and Crowe, D.L. (2008). Extracellular signals regulate rapid coactivator recruitment at AP-1 sites by altered phosphorylation of both CREB binding protein and c-jun. Mol. Cell. Biol. *28*, 4240–4250.

Tyssowski, K.M., DeStefino, N.R., Cho, J.H., Dunn, C.J., Poston, R.G., Carty, C.E., Jones, R.D., Chang, S.M., Romeo, P., Wurzelmann, M.K., et al. (2018). Different neuronal activity patterns induce different gene expression programs. Neuron *98*, 530–546.e11.

Tzschentke, T.M. (2007). Measuring reward with the conditioned place preference (CPP) paradigm: update of the last decade. Addict. Biol. *12*, 227–462.

Vialou, V., Feng, J., Robison, A.J., Ku, S.M., Ferguson, D., Scobie, K.N., Mazei-Robison, M.S., Mouzon, E., and Nestler, E.J. (2012). Serum response factor and cAMP response element binding protein are both required for cocaine induction of ΔFosB. J. Neurosci. *32*, 7577–7584.

Vo, N., and Goodman, R.H. (2001). CREB-binding protein and p300 in transcriptional regulation. J. Biol. Chem. *276*, 13505–13508.

Xing, J., Ginty, D.D., and Greenberg, M.E. (1996). Coupling of the RAS-MAPK pathway to gene activation by RSK2, a growth factor-regulated CREB kinase. Science *273*, 959–963.

Xing, J., Kornhauser, J.M., Xia, Z., Thiele, E.A., and Greenberg, M.E. (1998). Nerve growth factor activates extracellular signal-regulated kinase and p38 mitogen-activated protein kinase pathways to stimulate CREB serine 133 phosphorylation. Mol. Cell. Biol. *18*, 1946–1955.

Yoshihara, S., Takahashi, H., Nishimura, N., Kinoshita, M., Asahina, R., Kitsuki, M., Tatsumi, K., Furukawa-Hibi, Y., Hirai, H., Nagai, T., et al. (2014). Npas4 regulates Mdm2 and thus Dcx in experience-dependent dendritic spine development of newborn olfactory bulb interneurons. Cell Rep. *8*, 843–857.

Yoshimura, T., Kawano, Y., Arimura, N., Kawabata, S., Kikuchi, A., and Kaibuchi, K. (2005). GSK-3beta regulates phosphorylation of CRMP-2 and neuronal polarity. Cell *120*, 137–149.

Yun, J., Koike, H., Ibi, D., Toth, E., Mizoguchi, H., Nitta, A., Yoneyama, M., Ogita, K., Yoneda, Y., Nabeshima, T., et al. (2010). Chronic restraint stress impairs neurogenesis and hippocampus-dependent fear memory in mice: possible involvement of a brain-specific transcription factor Npas4. J. Neurochem. *114*, 1840–1851.

Yun, J., Nagai, T., Furukawa-Hibi, Y., Kuroda, K., Kaibuchi, K., Greenberg, M.E., and Yamada, K. (2013). Neuronal Per Arnt Sim (PAS) domain protein 4 (NPAS4) regulates neurite outgrowth and phosphorylation of synapsin I. J. Biol. Chem. *288*, 2655–2664.

STAR★METHODS

KEY RESOURCES TABLE

REAGENT or RESOURCE	SOURCE	IDENTIFIER
Antibodies		
Rabbit monoclonal anti-phospho-CREB (S133)	Cell Signaling Technology	Cat# 9198; RRID: AB_2561044
Rabbit monoclonal anti-CREB	Cell Signaling Technology	Cat# 9197; RRID: AB_331277
Mouse monoclonal anti-CREB	Cell Signaling Technology	Cat# 9104; RRID: AB_490881
Rabbit monoclonal anti-Histone H3	Cell Signaling Technology	Cat# 4499; RRID: AB_10544537
Rabbit monoclonal anti-FosB	Cell Signaling Technology	Cat# 2251; RRID: AB_2106903
Rabbit monoclonal anti-phospho-p44/42 MAPK (ERK1/2) (T202/Y204)	Cell Signaling Technology	Cat# 4370; RRID: AB_2315112
Rabbit monoclonal anti-p44/42 MAPK (ERK1/2)	Cell Signaling Technology	Cat# 4695; RRID: AB_390779
Mouse monoclonal anti-p44/42 MAPK (ERK1/2)	Cell Signaling Technology	Cat# 9107; RRID: AB_10695739
Rabbit monoclonal anti-phospho-SAPK/JNK (T183 / Y185)	Cell Signaling Technology	Cat# 4668; RRID: AB_823588
Rabbit polyclonal anti-SAPK/JNK	Cell Signaling Technology	Cat# 9252; RRID: AB_2250373
Rabbit monoclonal anti-phospho-p38 MAPK (T180/Y182)	Cell Signaling Technology	Cat# 4631; RRID: AB_331765
Mouse monoclonal p38 MAPK	Cell Signaling Technology	Cat# 9217; RRID: AB_331298
Rabbit monoclonal anti-phospho-AKT (T308)	Cell Signaling Technology	Cat# 2965; RRID: AB_2255933
Rabbit monoclonal anti-AKT	Cell Signaling Technology	Cat# 4691; RRID: AB_915783
Rabbit polyclonal anti-Npas4	Merck	Cat# HPA039255; RRID: AB_10674282
Mouse monoclonal anti-CBP/p300	Merck	Cat# P2859; RRID: AB_260994
Rabbit polyclonal anti-Rasgrp2	Thermo Fisher Scientific	Cat# PA5-35111; RRID: AB_2552421
Rabbit polyclonal anti-Mkl2	Novus Biologicals	Cat# NBP1-46209; RRID: AB_10009441
Mouse monoclonal anti-Jun	BD Biosciences	Cat# 610327; RRID: AB_397717
Mouse monoclonal anti-CRMP-2	IBL-America	Cat# JP11096; RRID: AB_1630812
Rabbit polyclonal anti-Matrin-3	Bethyl Laboratories	Cat# A300-591A; RRID: AB_495514
Rabbit polyclonal anti-Pur-alpha	Abcam	Cat# ab79936; RRID: AB_2253242
Rabbit polyclonal anti-CBP (A-22)	Santa Cruz Biotechnology	Cat# sc-369; RRID: AB_631006
Rabbit polyclonal anti-c-Myc (A-14)	Santa Cruz Biotechnology	Cat# sc-789; RRID: AB_631274
Rabbit polyclonal anti-RFP	MBL International	Cat# PM005; RRID: AB_591279
Rabbit polyclonal anti-GFP	MBL International	Cat# 598; RRID: AB_591819
Mouse monoclonal anti-GFP	Roche	Cat# 11814460001; RRID: AB_390913
Rat monoclonal anti-GFP	Nacalai Tesque	Cat# GF090R; RRID: AB_2314545
Mouse monoclonal anti-GST	FUJIFILM Wako	Cat# 017-21854
Rabbit polyclonal anti-phospho-CRMP2 (T514)	Yoshimura et al., 2005	N/A
Rabbit polyclonal anti-phospho-Rasgrp2 (S116/S117)	Nagai et al., 2016	N/A
Rabbit polyclonal anti-Npas4	Yun et al., 2010	N/A
Rabbit polyclonal anti-phospho-Npas4 (T427)	This paper	N/A
Rabbit polyclonal anti-phospho-Npas4 (S577)	This paper	N/A
Rabbit polyclonal anti-phospho-Npas4 (S580)	This paper	N/A
Rabbit polyclonal anti-phospho-Npas4 (S615)	This paper	N/A
Donkey anti-Rat IgG, Alexa Fluor 488	Thermo Fisher Scientific	Cat# A-21208; RRID: AB_2535794
Donkey anti-Rabbit IgG, Alexa Fluor 555	Thermo Fisher Scientific	Cat# A-31572; RRID: AB_162543
Donkey anti-Mouse IgG, Alexa Fluor 647	Thermo Fisher Scientific	Cat# A-31571; RRID: AB_162542
Goat anti-rabbit IgG, Alexa Fluor 680	Thermo Fisher Scientific	Cat# A-21109; RRID: AB_2535758
Goat anti-Mouse IgG, Alexa Fluor 680	Thermo Fisher Scientific	Cat# A-21058; RRID: AB_2535724

(*Continued on next page*)

Continued

REAGENT or RESOURCE	SOURCE	IDENTIFIER
anti-mouse IgG (DyLight 800 Conjugate)	Cell Signaling Technology	Cat# 5257; RRID: AB_10693543
IRDye 800CW Goat anti-Mouse IgG	LI-COR Biosciences	Cat# 925-32210; RRID: AB_2687825
Bacterial and Virus Strains		
pAAV-Sp-Cre	Hikida et al., 2010; Nagai et al., 2016	N/A
pAAV-Sp-EGFP	Hikida et al., 2010; Nagai et al., 2016	N/A
pAAV-CAGGS-Flex-EGFP-P2A-MCS-WPRE	Nagai et al., 2016	N/A
pAAV-CAGGS-Flex-EGFP-P2A-dnMAP2K1-WPRE	Nagai et al., 2016	N/A
pAAV-CaMKII-Flex-mCherry-P2A-MCS-WPRE	This paper	N/A
pAAV-CaMKII-Flex-mCherry-P2A-Npas4-WT-WPRE	This paper	N/A
pAAV-CaMKII-Flex-mCherry-P2A-Npas4-6A-WPRE	This paper	N/A
pAAV-CaMKII-Flex-mCherry-P2A-Npas4-6E-WPRE	This paper	N/A
pAAV-CaMKII-Flex-mCherry-P2A-Npas4-DN-WPRE	This paper	N/A
Chemicals, Peptides, and Recombinant Proteins		
Okadaic acid	LC Laboratories	Cat# O-5857
Forskolin [7β-Acetoxy-8,13-epoxy-1α,6β,9α-trihydroxy-labd-14-en-11-one]	Merck	Cat# 344270
U0126 [1,4-diamino-2,3-dicyano-1,4-bis (o-aminophenylmercapto) butadiene]	Merck	Cat# 662005
SP600125 [Anthra[1,9-cd]pyrazol-6(2H)-one,1,9-pyrazoloanthrone]	Merck	Cat# S5567
H-89 Dihydrochloride N-[2-((p-Bromocinnamyl) amino) ethyl]-5-isoquinolinesulfonamide, 2HCl,	Merck	Cat# 371962
LY294002 [2-(4-Morpholinyl)-8-phenyl-1(4H)-benzopyran-4-one]	Merck	Cat# 440202
SB203580 [4-(4-Fluorophenyl)-2-(4-methylsulfinylphenyl)-5-(4-pyridyl)1H-imidazole]	Tocris Bioscience	Cat# 1202/1
SB216763 [3-(2,4-Dichlorophenyl)-4-(1-methyl-1H-indol-3-yl)-1H-pyrrole-2,5-dione]	Tocris Bioscience	Cat# 1616
cOmplete, Mini, EDTA-free Protease Inhibitor Cocktail	Roche	Cat# 11836170001
PhosSTOP	Roche	Cat# 04906837001
Lipofectamine 2000	Thermo Fisher Scientific	Cat# 11668500
Dulbecco's Modified Eagle's Medium (DMEM)	Merck	Cat# D5796
Fetal Bovine Serum (FBS)	Merck	Cat# 173012
Neurobasal medium	Thermo Fisher Scientific	Cat# 21103049
B-27 supplement	Thermo Fisher Scientific	Cat# 17504044
GlutaMax Supplement	Thermo Fisher Scientific	Cat# 35050061
Poly-D-lysine hydrobromide	Merck	Cat# P6407
Neuron Dissociation Solutions	FUJIFILM Wako	Cat# 297-78101
Glutathione Sepharose 4B	GE Healthcare	Cat# 217075605
Trypsin/Lys-C Mix	Promega	Cat# V5072
Glu-C	Promega	Cat# V1651
Asp-N	FUJIFILM Wako	Cat# 056-05921
2,2,2-Tribromoethanol (Avertin)	FUJIFILM Wako	Cat# 203-14602
Tert-amylalcohol (Avertin)	FUJIFILM Wako	Cat# 010-03703
active MAPK1	Carna Biosciences	Cat# 204-143
GST-CBP-RID	This paper	N/A
GST-CBP-N-TAD	This paper	N/A
GST-CBP-bromo	This paper	N/A
GST-CBP-HAT	This paper	N/A

(*Continued on next page*)

Continued

REAGENT or RESOURCE	SOURCE	IDENTIFIER
GST-CBP-C-TAD	This paper	N/A
GST-Npas4 1-273 aa	This paper	N/A
GST-Npas4 274-597 aa	This paper	N/A
GST-Npas4 598-802 aa	This paper	N/A
Critical Commercial Assays		
Dual-Luciferase Reporter Assay System	Promega	Cat# E1910
Nuclear Extract Kit	Active Motif	Cat# 40010
PrimeSTAR Mutagenesis Basal Kit	Takara	Cat# R046A
Experimental Models: Cell Lines		
COS7 cell line	ATCC	RRID: CVCL_0224
AAV293 cell line	Cell BioLabs	RRID: CVCL_KA64
Cultured striatal neurons (from embryos of ICR mice)	Cowan et al., 2005	N/A
Experimental Models: Organisms/Strains		
C57BL/6	Japan SLC	RRID: IMSR_JAX:000664
ICR	Japan SLC	RRID: IMSR_JAX:009122
Npas4 KO (Npas4tm1Meg/Npas4tm1Meg)	Lin et al., 2008	RRID: MGI:3828101
Npas4 flox (Npas4tm2Meg/Npas4tm2Meg)	Lin et al., 2008	RRID: MGI:3828102
Drd1-mVenus (C57BL/6J-Tg (mDrd1-YFP) 680-1Koba/KobaRbrc)	Nagai et al., 2016	RRID: IMSR_RBRC03111
Drd2-mVenus (C57BL/6J-Tg (Drd2-YFP) 364-5Koba/KobaRbrc)	Nagai et al., 2016	RRID: IMSR_RBRC02332
B6. FVB (Cg)-Tg (Drd1a-cre) EY262Gsat/Mmucd	GENSAT (Gong et al., 2003)	RRID: MMRRC_030989-UCD
B6. FVB (Cg)-Tg (Adora2a-cre) KG139Gsat/Mmucd	GENSAT (Gong et al., 2003)	RRID: MMRRC_036158-UCD
Recombinant DNA		
pCAGGS-Myc-MAP2K1 (MEK1)-WT	Funahashi et al., 2013	N/A
pCAGGS-Myc-MAP2K1 (MEK1)-CA	Funahashi et al., 2013	N/A
pCAGGS-Myc-MAP2K1 (MEK1)-DN	Funahashi et al., 2013	N/A
Human CBP cDNA	Kazusa DNA Research Institute	Cat# ORK11778
Mouse Npas4 cDNA	Yun et al., 2013	N/A
pENTR/D-TOPO	Thermo Fisher Scientific	Cat# K240020
pDEST15	Thermo Fisher Scientific	Cat# 11802014
pDEST15-CBP-RID	This paper	N/A
pDEST15-CBP-N-TAD	This paper	N/A
pDEST15-CBP-bramo	This paper	N/A
pDEST15-CBP-HAT	This paper	N/A
pDEST15-CBP-C-TAD	This paper	N/A
pDEST15-Npas4 1-273 aa	This paper	N/A
pDEST15-Npas4 274-597 aa	This paper	N/A
pDEST15-Npas4 598-802 aa	This paper	N/A
pCAGGS-Myc-CBP-N-TAD	This paper	N/A
pEF-BOS-GST	This paper	N/A
pEF-BOS-GST-CBP-N-TAD	This paper	N/A
pEF-BOS-GST-Npas4-390-489 aa	This paper	N/A
pEF-BOS-GST-Npas4-490-597 aa	This paper	N/A
pEF-BOS-GST-Npas4-598-701 aa	This paper	N/A
pcDNA-mGFP	This paper	N/A
pcDNA-mGFP-Npas4-WT	This paper	N/A
pcDNA-mGFP-Npas4-T423A	This paper	N/A

(*Continued on next page*)

Continued

REAGENT or RESOURCE	SOURCE	IDENTIFIER
pcDNA-mGFP-Npas4-T427A	This paper	N/A
pcDNA-mGFP-Npas4-S577A	This paper	N/A
pcDNA-mGFP-Npas4-S580A	This paper	N/A
pcDNA-mGFP-Npas4-T611A	This paper	N/A
pcDNA-mGFP-Npas4-S615A	This paper	N/A
pcDNA-mGFP-Npas4-T423A/T427A/S577A/S580A/ T611A/S615A (6A)	This paper	N/A
pcDNA-mGFP-Npas4-T423E/T427E/S577E/S580E/ T611E/S615E (6E)	This paper	N/A
pcDNA-mGFP-Npas4-274-389 aa	This paper	N/A
pcDNA-mGFP-Npas4-390-489 aa	This paper	N/A
pcDNA-mGFP-Npas4-490-597 aa	This paper	N/A
pcDNA-mGFP-Npas4-598-701 aa	This paper	N/A
pcDNA-mGFP-Npas4-701-802 aa	This paper	N/A
pcDNA-mGFP-Npas4-390-489 aa-T423A	This paper	N/A
pcDNA-mGFP-Npas4-390-489 aa-T427A	This paper	N/A
pcDNA-mGFP-Npas4-390-489 aa-T423A/T427A	This paper	N/A
pcDNA-mGFP-Npas4-490-597 aa-S577A	This paper	N/A
pcDNA-mGFP-Npas4-490-597 aa-S580A	This paper	N/A
pcDNA-mGFP-Npas4-490-597 aa-S577A/S580A	This paper	N/A
pcDNA-mGFP-Npas4-598-701 aa-T611A	This paper	N/A
pcDNA-mGFP-Npas4-598-701 aa-S615A	This paper	N/A
pcDNA-mGFP-Npas4-598-701 aa-T611A/S615A	This paper	N/A
pGL4.31 [luc2P/GAL4 UAS/Hygro] Vector	Promega	Cat# C9351
pGL4.15 [luc2P/Hygro] Vector	Promega	Cat# E6701
pGL4.74 [hRluc/TK] Vector	Promega	Cat# E6921
pFN11 (BIND) Flexi Vector	Promega	Cat# C9341
pGL4.15-exon1 BDNF promoter	This paper	N/A
pFN11A (BIND)-Npas4-274-802 aa	This paper	N/A
pAAV-Sp-Cre	Hikida et al., 2010; Nagai et al., 2016	N/A
pAAV-Sp-EGFP	Hikida et al., 2010; Nagai et al., 2016	N/A
pAAV-CAGGS-Flex-EGFP-P2A-MCS-WPRE	Nagai et al., 2016	N/A
pAAV-CAGGS-Flex-EGFP-P2A-MAP2K1-DN-WPRE	Nagai et al., 2016	N/A
pAAV- CaMKII-Flex-mCherry-P2A-MCS-WPRE	This paper	N/A
pAAV- CaMKII-Flex-mCherry-P2A-Npas4-WT-WPRE	This paper	N/A
pAAV- CaMKII-Flex-mCherry-P2A-Npas4-6A-WPRE	This paper	N/A
pAAV- CaMKII-Flex-mCherry-P2A-Npas4-6E-WPRE	This paper	N/A
pAAV- CaMKII-Flex-mCherry-P2A-Npas4-DN-WPRE	This paper	N/A
pHelper	Cell BioLabs	Cat# 340202
pAAV-DJ	Cell BioLabs	Cat# VPK-420-DJ
Software and Algorithms		
Prism 6	GraphPad	RRID: SCR_002798
Proteome Discoverer 1.4	Thermo Fisher Scientific	RRID: SCR_014477
Mascot	Matrix Science	RRID: SCR_014322
DAVID bioinformatics resources	Huang da et al., 2009a, 2009b	https://david.ncifcrf.gov
ZEN Digital Imaging for Light Microscopy	Carl Zeiss	RRID: SCR_013672
LI-COR Image Studio Software	LI-COR Biosciences	RRID: SCR_015795
Gen5 software	BioTek	RRID: SCR_017317

(*Continued on next page*)

Continued

REAGENT or RESOURCE	SOURCE	IDENTIFIER
MED-PC IV software	MED Associates	RRID: SCR_012156
Adobe Photoshop CS6	Adobe	RRID: SCR_014199
Adobe Illustrator CS6	Adobe	RRID: SCR_010279
Other		
Identification of CBP-interacting proteins by LC-MS/MS	This paper	https://dx.doi.org/10.17632/gh228m9gms.2
Identification of phosphorylation site of Npas4 by LC-MS/MS	This paper	https://dx.doi.org/10.17632/3f5p2p7hbs.2

LEAD CONTACT AND MATERIALS AVAILABILITY

Further information and requests for resources and reagents should be directed to and will be fulfilled by the Lead Contact, Kozo Kaibuchi (kaibuchi@med.nagoya-u.ac.jp).

All unique/stable reagents generated in this study will be made available on request but we may require a payment and/or a completed Materials Transfer Agreement if there is potential for commercial application.

EXPERIMENTAL MODEL AND SUBJECT DETAILS

Animals

C57BL/6 (RRID: IMSR_JAX:000664) and ICR (RRID: IMSR_JAX:009122) mice were purchased from Japan SLC (Shizuoka, Japan). Npas4 KO (RRID: MGI:3828101) and Npas4 flox (RRID: MGI:3828102) mice on a C57BL/6 genetic background were kindly provided by Dr. Michael E. Greenberg (Harvard Medical School, Boston, MA, USA) and have been previously described (Lin et al., 2008). Drd1-mVenus (C57BL/6J-Tg (mDrd1-YFP) 680-1Koba/KobaRbrc, RRID: IMSR_RBRC03111) and Drd2-mVenus transgenic mice (C57BL/6J-Tg (Drd2-YFP) 364-5Koba/KobaRbrc, RRID: IMSR_RBRC02332) were generated as previously described (Nagai et al., 2016). Drd1a-Cre mice on a C57BL/6 background (B6. FVB (Cg)-Tg (Drd1a-cre) EY262Gsat/Mmucd, RRID: MMRRC_030989-UCD) and Adora2a-Cre mice on a C57BL/6 background (B6. FVB (Cg)-Tg (Adora2a-cre) KG139Gsat/Mmucd, RRID: MMRRC_036158-UCD) were provided by the Mutant Mouse Research and Resource Center (MMRRC) at UC Davis (Davis, CA, USA). Heterozygous Drd1a-Cre and Adora2a-Cre male mice were obtained by crossing heterozygous or homozygous Drd1a-Cre and Adora2a-Cre male mice with C57BL/6 female mice. Mice were housed under a standard 12-h light/dark cycle (light phase 9:00-21:00) at a constant temperature of 23 ± 1°C with free access to food and water throughout the experiments. The male mice used in this study were 7–12 weeks old and 22–29 g body weight unless otherwise indicated. All animal experiments were approved and performed in accordance with the guidelines for the care and use of laboratory animals established by the Animal Experiments Committee of Nagoya University Graduate School of Medicine.

Cell Lines

COS7 (Species: *Cercopithecus aethiops*, Sex: male, RRID: CVCL_0224, ATCC, Manassas, VA, USA) and AAV293 (Species: *Homo sapiens*, Sex: female, RRID: CVCL_KA64, Cell BioLabs, San Diego, CA, USA) cell lines were cultured in Dulbecco's modified Eagle's medium (DMEM) (Merck, Kenilworth, NJ, USA) containing 10% fetal bovine serum (FBS; Merck). Cells were grown in a humidified atmosphere of 5% CO_2 at 37°C.

Primary Cell Cultures

Primary cultured striatal neurons were prepared from E15-16 mouse embryos of ICR female mice (Japan SLC) as described previously (Cowan et al., 2005) with modifications. The striatal tissues were digested with neuron dissociation solutions (FUJIFILM Wako, Tokyo, Japan) according to the manufacturer's instructions. Dissociated neurons were seeded on coverslips or dishes coated with poly-D-lysine (PDL; Merck) and cultured in Neurobasal medium (Thermo Fisher Scientific, Waltham, MA, USA) containing 10% FBS (Merck). One hour after plating, the medium was changed to Neurobasal medium containing B-27 supplement (Thermo Fisher Scientific) and 1 mM GlutaMAX (Thermo Fisher Scientific). Neurons were grown in a humidified atmosphere of 5% CO_2 at 37°C.

METHOD DETAILS

Materials

The cDNA encoding human CBP (ID: ORK11778) was purchased from Kazusa DNA Research Institute (Chiba, Japan). The cDNA encoding mouse Npas4 (GenBank: BC129861) was obtained as previously described (Yun et al., 2013). Rabbit polyclonal antibody against Npas4 phosphorylated at T427 (anti-pT427 antibody) was produced against the phosphopeptide CTPPYpT^{427}PHQPG

(Merck). Rabbit polyclonal antibody against Npas4 phosphorylated at S577, S580 and S615 (anti-pT427, anti-pS577 and pS580 antibodies) were produced against the phosphopeptides CEKLPPpS^{577}PSSPG, CPPSPSpS^{580}PGNGD and CLTPEApS^{615}PVKQS (FUJIFILM Wako, Tokyo, Japan). Rabbit polyclonal anti-Npas4 antibody was produced against GST-Npas4-C-term (Yun et al., 2010). Rabbit polyclonal anti-phospho-CRMP2 (T514) antibody was obtained as previously described (Yoshimura et al., 2005). Rabbit polyclonal anti-phospho-Rasgrp2 (S116/S117) antibody was obtained as previously described (Nagai et al., 2016). The following antibodies and materials were used: rabbit polyclonal anti-CBP (A-22) (RRID: AB_631006) and rabbit polyclonal anti-c-Myc (A-14) (RRID: AB_631274) antibodies (Santa Cruz, Dallas, TX, USA); Rabbit monoclonal anti-phospho-CREB (S133) (RRID: AB_2561044), rabbit monoclonal anti-CREB (RRID: AB_331277), mouse monoclonal anti-CREB (RRID: AB_490881), rabbit monoclonal anti-Histone H3 (RRID: AB_10544537), rabbit monoclonal anti-FosB (RRID: AB_2106903), rabbit monoclonal anti-phospho-p44/42 MAPK (ERK1/2) (T202/Y204) (RRID: AB_2315112), rabbit monoclonal anti-p44/42 MAPK (ERK1/2) (RRID: AB_390779), mouse monoclonal anti-p44/42 MAPK (ERK1/2) (RRID: AB_10695739), rabbit monoclonal anti-phospho-SAPK/JNK (T183/Y185) (RRID: AB_823588), rabbit polyclonal anti-SAPK/JNK (RRID: AB_2250373) rabbit monoclonal anti-phospho-p38 MAPK (T180/Y182), mouse monoclonal p38 MAPK (RRID: AB_331298), rabbit monoclonal anti-phospho-AKT (T308) (RRID: AB_2255933), rabbit monoclonal anti-AKT (RRID: AB_915783) antibodies (Cell Signaling Technology Inc, Danvers, MA, USA); rabbit polyclonal anti-Npas4 (RRID: AB_10674282), mouse monoclonal anti-CBP/p300 (RRID:AB_260994) antibodies (Merck); rabbit polyclonal anti-GFP (RRID: AB_591819) and rabbit polyclonal anti-RFP (RRID: AB_591279) antibodies (MBL International, Aichi, Japan); mouse monoclonal anti-GFP antibody (RRID: AB_390913, Roche, Mannheim, Germany); mouse monoclonal anti-GST antibody (FUJIFILM Wako); rabbit polyclonal anti-Rasgrp2 antibody (RRID: AB_254634, Thermo Fisher Scientific); mouse monoclonal anti-Jun antibody (RRID: AB_397717, BD Biosciences, CA, USA) ; rabbit polyclonal anti-Mkl2 antibody (RRID: AB_10009441, Novus Biologicals, Littleton, CO, USA); rabbit polyclonal anti-Matrin-3 antibody (RRID: AB_495514, Bethyl Laboratories, Montgomery, TX, USA); rabbit polyclonal anti-Pur-alpha antibody (RRID: AB_2253242, Abcam, Cambridge, UK); Alexa 488-, Alexa 555- and Alexa 647- conjugated secondary antibodies against rat, rabbit or mouse immunoglobulin, respectively (RRID: AB_2535794, RRID: AB_162543, RRID: AB_2535758, Thermo Fisher Scientific); active MAPK1 (Carna Biosciences, Kobe, Japan); Okadaic acid (OA) (LC Laboratories, Woburn, MA, USA); Forskolin [7β-Acetoxy-8,13-epoxy-1α,6β,9α-trihydroxy-labd-14-en-11-one], MAP2K1/2 inhibitor U0126 [1,4-diamino-2,3-dicyano-1,4-bis (o-aminophenylmercapto) butadiene], JNK Inhibitor II SP600125 [Anthra [1,9-cd] pyrazol-6 (2H)-one,1,9-pyrazoloanthrone], and PKA inhibitor H-89 Dihydrochloride N-[2-((p-Bromocinnamyl)amino)ethyl]-5-isoquinolinesulfonamide, 2HCl, and PI3K inhibitor LY294002 [2-(4-Morpholinyl)-8-phenyl-1(4H)-benzopyran-4-one] (Merck). p38 MAPK inhibitor SB203580 [4-(4-Fluorophenyl)-2-(4-methylsulfinylphenyl)-5-(4-pyridyl)1H-imidazole] and GSK3 inhibitor SB216763 [3-(2,4-Dichlorophenyl)-4-(1-methyl-1H-indol-3-yl)-1H-pyrrole-2,5-dione] (Tocris Bioscience, Cambridge, UK). Other materials and chemicals were obtained from commercial sources.

Plasmid Constructs

We subcloned the PCR-amplified cDNA fragments of Npas4 and CBP into pENTR-D/TOPO (Thermo Fisher Scientific). After sequencing, these fragments were further subcloned into appropriate commercial or homemade destination vectors via Gateway technology (Thermo Fisher Scientific) according to the manufacturer's instructions. The mutants Npas4-T423A, Npas4-T427A, Npas4-S577A, Npas4-S580A, Npas4-T611A, Npas4-S615A, Npas4-6A and Npas4-6E were generated with a PrimeSTAR Mutagenesis Basal Kit (Takara, Shiga, Japan) by changing T423, T427, S577, S580, T611 and/or S615 into alanine or glutamic acid. The exon 1 BDNF promoter region was amplified with primer pair [5′-CCATTAGAGCAAACGCAGTCATA-3′ (forward), 5′ CCACCACTTGGTGT GACTTATG-3′ (reverse)] using mouse genomic DNA and subcloned into the pGL4.15 [luc2P/Hygro] vector (Promega, Madison, WI, USA). pCAGGS-Myc-MAP2K1-WT, -CA and -DN were obtained as previously described (Funahashi et al., 2013). GST-tagged proteins were produced in BL21 (DE3) or Rosetta (DE3) *Escherichia coli* cells and purified on glutathione-Sepharose 4B beads (GE Healthcare, Chicago, IL, USA). To generate an AAV vector that bicistronically expresses the mCherry protein and the target protein in a Cre-dependent manner, we constructed the pAAV-CaMKII-Flex-mCherry-P2A-MCS-WPRE plasmid by modifying the pAAV-CAGGS-Flex-MCS-WPRE plasmid. We cloned the mCherry cDNA sequence, followed by a self-cleaving 2A peptide sequence and a multiple cloning site (MCS), into the MCS of pAAV-CAGGS-Flex-MCS-WPRE in an inverted manner. The CAGGS promoter was replaced with the CaMKII promoter. Npas4-WT, 6A, 6E or DN (deltaC 274-802 aa) were each cloned into the MCS of the pAAV-CaMKII-Flex-mCherry-P2A-MCS-WPRE plasmid. pAAV-Sp-EGFP, pAAV-Sp-Cre, pAAV-CAGGS-Flex-EGFP-P2A-MCS-WPRE, and pAAV-CAGGS-Flex-EGFP-P2A-MAP2K1-DN-WPRE were generated as previously described (Nagai et al., 2016).

Laemmli's SDS-PAGE, Phos-tag SDS-PAGE, and Immunoblotting

Laemmli's SDS-PAGE was carried out using 6%, 8% or 10% polyacrylamide gels (Nacalai Tesque, Kyoto, Japan). Phos-tag SDS-PAGE was performed with 6%, 7.5% or 10% polyacrylamide gels containing 25 μM Phos-tag acrylamide (FUJIFILM Wako) and 75 μM $MnCl_2$. The proteins were separated via SDS-PAGE and transferred to polyvinylidene difluoride membranes (Immobilon-FL, Merck). The membranes were blocked for 30 min with Blocking-One or Blocking-One P (Nacalai Tesque) and incubated for 1 hr at room temperature or overnight at 4 °C with primary antibodies. After the membranes were washed, they were incubated for 30 min with goat anti-rabbit IgG Alexa Fluor 680 (RRID: AB_2535758, Thermo Fisher Scientific), goat anti-Mouse IgG, Alexa Fluor 680 (RRID: AB_2535724, Thermo Fisher Scientific) or anti-mouse IgG DyLight 800 Conjugate (RRID: AB_10693543, Cell Signaling Technology) at room temperature for 30 min. Specific binding was detected using an infrared (LI-COR Biosciences, Lincoln, NE) imaging system. Band intensities were quantified using ImageStudio software (RRID: SCR_015795, LI-COR Biosciences).

In Vitro Phosphorylation Assay

The phosphorylation assay was performed as previously described (Amano et al., 2015; Funahashi et al., 2013). Npas4 fragments were expressed in *E. coli* as GST fusion proteins and purified with glutathione-Sepharose 4B beads (GE Healthcare). The kinase reactions for MAPK1 were performed in 100 μl of a reaction mixture (50 mM Tris/HCl, pH 7.5, 1 mM EDTA, 1 mM EGTA, 1 mM DTT, 5 mM $MgCl_2$, 50 μM [Γ32P] ATP [1-20 GBq/mmol]), 0.05 μM active MAPK1, and 0.3 μM purified GST-Npas4 fragments for 30 min at 30°C. Then, the reaction mixtures were boiled in SDS sample buffer and subjected to SDS-PAGE and silver staining. The radiolabeled proteins were visualized with an image analyzer (FLA9000; GE Healthcare).

GST Pulldown Assay

For determining the binding site between CBP and Npas4, COS7 cells were transfected GFP-Npas4-WT or Myc-CBP-N-TAD. After 18-24 hr transfection, cells were lysed in lysis buffer [20 mM Tris/HCl, 1 mM EDTA, 150 mM NaCl, 1% NP-40, protease inhibitor cocktail (Roche), and phosphatase inhibitor cocktail (PhosStop, Roche), pH 7.5] and sonicated 3 times for 5 s. After centrifugation at 16,000 × g at 4°C for 10 min, the soluble supernatant was incubated with glutathione-Sepharose 4B beads coated with 100 pmol of GST, GST-CBP or GST-Npas4 fragments for 1 hr at 4°C with gentle rocking. For the interaction assay of exogenous CBP and Npas4, COS7 cells were transfected with the indicated plasmids. After 18-24 hr transfection, cells were pretreated with the indicated kinase inhibitors and then treated with DMSO or OA. Cells were lysed in lysis buffer containing protease inhibitor cocktail and PhosStop, and then sonicated 3 times for 5 s. After centrifugation at 16,000 × g at 4°C for 10 min, the soluble supernatant was incubated in 30 μl of glutathione-Sepharose 4B beads for 1 hr at 4°C with gentle rocking. The beads were washed three times with lysis buffer, eluted by boiling in SDS sample buffer for SDS-PAGE and then subjected to immunoblot analysis with the indicated antibodies.

Mass Spectrometry

For identification of CBP-interacting proteins, after CPP conditioning for 30 min, brains from 10 mice were rapidly removed and coronal slices (1 mm) were produced using a mouse brain slicer matrix (Brain Science Idea Co., Ltd., Osaka, Japan). The striatum and NAc (approximately +1.54 mm from Bregma) were collected using 3 mm diameter biopsy punch (Miltex, NY, USA) based on the Paxinos and Franklin ''the mouse brain in stereotaxic coordinates.'' Collected tissues were homogenized with Hypotonic buffer (Nuclear Extract Kit, Active Motif, CA, USA) containing protease inhibitor cocktail and PhosStop using potter homogenizer and incubated on ice for 15 min. The lysate was centrifuged at 800 × g for 10 min at 4°C. The pellet was resuspended with Hypotonic buffer and incubated on ice for 15 min. After addition of a detergent and vortexing for 10 s, the lysate was centrifuged at 16,000 × g for 2 min. The nuclear pellet was extracted in lysis buffer containing protease inhibitor cocktail and PhosStop, and then sonicated 3 times for 10 s. The lysate was centrifuged at 16,000 × g for 10 min at 4°C. The supernatant was used as the nuclear extracts. A total of 250 pmol of GST or GST-CBP-N-TAD, immobilized on glutathione Sepharose 4B beads, was incubated with the nuclear extracts for 1 hr at 4°C with rotation. The beads were then washed three times with Lysis buffer and an additional three times with wash buffer (20 mM Tris/HCl, 1 mM EDTA, and 150 mM NaCl, pH 7.5) to remove the detergent from the beads.

For identification of Npas4 phosphorylation site, GST-Npas4 fragment was expressed in COS7 cells with or without the coexpression of MAP2K1-CA. Cells were lysed in lysis buffer containing protease inhibitor cocktail (Roche) and PhosStop (Roche), and sonicated 3 times for 5 s. After centrifugation at 16,000 × g at 4°C for 10 min, the soluble supernatant was incubated in 30 μl of glutathione-Sepharose 4B beads for 1 hr at 4°C with rotation. The beads were then washed three times with lysis buffer and an additional three times with wash buffer.

The bound proteins were extracted from the beads using urea solution (1 M urea and 50 mM NH4HCO3), reduced via incubation in 5 mM dithiothreitol for 30 min, and alkylated using 10 mM iodoacetamide for 1 hr in the dark. The proteins were digested with Trypsin/Lys-C (Promega) or Glu-C (Promega)/Asp-N (FUJIFILM Wako). Demineralization was performed using SPE c-tips (Nikkyo Technos, Tokyo, Japan) according to the manufacturer's instructions. The peptides were analyzed by LC−MS using an Orbitrap Fusion mass spectrometer (Thermo Fisher Scientific Inc) coupled to an UltiMate3000 RSLCnano LC system (Dionex Co., Amsterdam, the Netherlands) using a nano HPLC capillary column, 150 mm × 75 m i.d (Nikkyo Technos Co., Tokyo, Japan) via a nanoelectrospray ion source.

Reversed-phase chromatography was performed with a linear gradient (0 min, 5% B; 100 min, 40% B) of solvent A (2% acetonitrile with 0.1% formic acid) and solvent B (95% acetonitrile with 0.1% formic acid) at an estimated flow rate of 300 nl/min. A precursor ion scan was carried out using a 400-1600 mass to charge ratio (m/z) prior to MS/MS analysis. Tandem MS was performed by isolation at 0.8 Th with the quadrupole, HCD fragmentation with normalized collision energy of 30%, and rapid scan MS analysis in the ion trap. Only those precursors with charge states of 2-6 were sampled for MS2. The dynamic exclusion duration was set to 10 s with a 10 ppm tolerance. The instrument was run in top speed mode with 3 s cycles.

Data Analysis for Mass Spectrometry

The raw data were processed using Proteome Discoverer 1.4 (RRID: SCR_014477, Thermo Fisher Scientific) in conjunction with the MASCOT search engine, version 2.6.0 (RRID: SCR_014322, Matrix Science Inc., Boston, MA) for protein identification. Peptides and proteins were identified against the mouse protein database in UniProt (release 2018_11), with a precursor mass tolerance of 10 ppm

and a fragment ion mass tolerance of 0.8 Da. Peptides were identified with the false discovery rate (FDR) < 1% (Identification of phosphorylation site of Npas4) or 5% (Screening of CBP-interacting protein). Fixed modification was set to cysteine carbamidomethylation, and variable modifications were set to methionine oxidation and serine, threonine tyrosine phosphorylation. Two missed cleavages by trypsin/Lys-C or Glu-C/Asp-N were allowed. Quantification was carried out by SIM analysis, to obtain the peak area values of dual phosphorylated peptides. Gene ontology (GO) analysis (biological process) and KEGG pathway analysis were performed using the DAVID bioinformatics resources (https://david.ncifcrf.gov)

Immunofluorescence Analysis

Mice were anesthetized with 2,2,2-tribromoethanol/tert-amyl alcohol solution (Avertin, 200 mg/kg, i.p.) (FUJIFILM Wako) for rapid and deep anesthesia and transcardially perfused with 4% paraformaldehyde. Then, the brains were removed and incubated in 4% paraformaldehyde overnight at 4 °C. The brains were sectioned coronally with a vibratome (VT1200S, Leica Microsystems, Wetzlar, Germany) at a thickness of 50 μm. The brain slices were incubated with 0.1% Triton X-100/phosphate-buffered saline (PBS) for 10 min and blocked with Blocking-One P for 30 min. Cultured striatal neurons were transfected with GFP-Npas4-WT at 7 days *in vitro* (DIV) using the Lipofectamine 2000 reagent (Thermo Fisher Scientific) according to the manufacturer's instructions. Neurons were treated with DMSO or 10 μM forskolin for 30 min at 8 DIV and fixed with 3.7% formaldehyde in PBS for 10 min at room temperature. Neurons were treatment with 0.05% Triton X-100/PBS for 10 min on ice and blocked with 10% donkey serum albumin in PBS. The brain slices and neurons were incubated with each indicated antibody overnight at 4°C or for 1hr at room temperature. After washing, the samples were incubated with Alexa Fluor 488-, Alexa Fluor 555- or Alexa Fluor 647-conjugated secondary antibodies for 1 hr. Nuclei were visualized by staining with Hoechst 33342 (Nacalai). Confocal images were recorded with LSM 780 microscopes built around an Axio Observer Z1 with Plan-Apochromat 20 × (numerical aperture [NA] 0.8), C-Apochromat 40 × (NA 1.2) or Plan-Apochromat 63 × (NA 1.40) lenses under the control of ZEN Digital Imaging for Light Microscopy (RRID: SCR_013672, Carl Zeiss, Oberkochen. Germany). The entire image of a coronal brain section was observed with a fluorescence microscope (BZ-9000 and BZ-X800, Keyence, Osaka, Japan).

Dual-Luciferase Reporter Assay

Striatal neurons were seeded on 24-well plates and cultured for 7-8 days. Neurons were cotransfected with pGL4-exon1 BDNF promoter or pGL4.31[luc2P/GAL4 UAS/Hygro] vector (Promega) and expression vectors using the Lipofectamine 2000 transfection reagent (Thermo Fisher Scientific) according to the manufacturer's instructions. As necessary, an empty control plasmid was added to ensure that each transfection received the same amount of total DNA. To normalize for transfection efficiency, we added pRluc-TK (*Renilla* luciferase) reporter plasmid (Promega) to each transfection. Luciferase activities were measured using a dual luciferase reporter assay system (Promega) and a PowerScan4 microplate reader (Bio Tek, Winooski, VT, USA). The data were analyzed using Gen5 software (RRID: SCR_017317, Bio Tek).

AAV Preparation and Injection

AAV vectors were prepared and titered as described previously (Sooksawate et al., 2013). Briefly, plasmids for the AAV vector, pHelper (Cell BioLabs), and pAAV-DJ (Cell BioLabs) were transfected into AAV293 cells. After 3 days of incubation, cells were collected and purified. The titers of AAV were estimated by qPCR. Mice were anesthetized with Avertin and positioned in a stereotaxic frame (David Kopf, Tujunga, CA, USA). An AAV virus (0.5 μL, 1.0×10^{12} genome copies/mL) was injected into the NAc through a glass microinjection capillary tube at a 10° angle and a rate of 0.1 μL/min (0.5 μL/site, four sites). The anteroposterior, mediolateral, and dorsoventral coordinates relative to bregma were as follows (in mm): +1.6, ± 1.5, and −4.4; and +1.0, ± 1.6, and −4.5.

Behavioral Analysis

The conditioned place preference test was performed as previously described (Nagai et al., 2016). The apparatus consisted of two compartments: a transparent Plexiglas box and a black Plexiglas box (W 16 cm × D 16 cm × H 17 cm). To be used as cues to enable the mice to distinguish between the boxes, the floor of the transparent box was covered with uneven Plexiglas and that of the black box was covered with smooth black Plexiglas. All sessions were conducted under conditions of dim illumination (40 lux). The place-conditioning schedule consisted of three phases: preconditioning, conditioning, and postconditioning. In the preconditioning phase, the mouse was allowed to move freely between the boxes for 30 min, twice a day. During the second session on day 1, the time spent in each of the boxes was measured for 15 min using MED-PC IV software (RRID: SCR_012156, Brainscience Idea, Osaka, Japan). Conditioning was counterbalanced between compartments to ensure that the procedure was unbiased. No initial place preference or aversion to either compartment was observed in the experiment. For 3 days, the mice were conditioned to an intraperitoneal saline injection in one chamber for 30 min during a morning session and to a 10 mg/kg intraperitoneal cocaine injection in the opposite chamber for 30 min during an afternoon session. Control animals received saline during every session. On day 5, the postconditioning phase was performed in a manner that was similar to the preconditioning phase, i.e., the mice were allowed free access to both compartments for 15 min, and the time spent in each of the boxes was measured. CPP was calculated for each mouse as the difference in the time spent on the cocaine-conditioned side between the pre- and postconditioning phases.

QUANTIFICATION AND STATISTICAL ANALYSIS

Data analysis was performed using Prism 6 Statistics software (RRID: SCR_002798, GraphPad Software, Inc., La Jolla, USA). All data are expressed as the means ± standard error of the mean (SEM). One-way or two-way analysis of variance (ANOVA) was used, followed by Tukey's or Dunnett's multiple-comparison test when the F ratios were significant ($p < 0.05$). Differences between two groups were tested for significance using t test.

DATA AND CODE AVAILABILITY

Relevant datasets for Table 1 and Figure 3E in the paper are available.
https://dx.doi.org/10.17632/gh228m9gms.2
https://dx.doi.org/10.17632/3f5p2p7hbs.2